https://doi.org/10.5194/egusphere-2026-2628
Preprint. Discussion started: 29 May 2026

Turbulence over the Atlantic ITCZ - Is the upper troposphere above doldrums less turbulent?

Andreas Dörnbrack[1], Andreas Giez[2], Christian Mallaun[2], and Claudia Christine Stephan[3]

[1]Institute of Atmospheric Physics, German Aerospace Center (DLR), Oberpfaffenhofen, Germany
[2]Flight Experiments, German Aerospace Center (DLR), Oberpfaffenhofen, Germany
[3]Leibniz Institute of Atmospheric Physics at the University of Rostock, Kühlungsborn, Germany

Correspondence: Andreas Dörnbrack (andreas.doernbrack@dlr.de)

Abstract. Flight level wind measurements from the German research aircraft HALO are used to investigate the turbulence in the upper troposphere over the inter-tropical convergence zone (ITCZ) of the eastern and western tropical Atlantic. During the 2024 PERCUSION mission, 23 research flights were conducted to investigate mesoscale drivers of the inner life cycle of the ITCZ and to provide a rich data set for validating EarthCARE satellite measurements. From these flights, 10 Hz BAHAMAS measurements along 183 constant altitude legs were extracted and analyzed to characterize the turbulence over the tropical Atlantic. A key focus was on investigating whether there is indeed a link between the recently discovered subsidence over the doldrums – calm regions within the ITCZ – and reduced turbulence activity in the upper troposphere. The ECMWF's meteorological analyses of 89 circular flight legs identified 13 doldrums in which the area-averaged wind speed at a height of 10 m was less than 3 m s^{-1}. These regions were further characterized by a column-integrated divergence, i.e. by mass spreading out above the doldrums.

The turbulence observed during the PERCUSION mission was generally stronger than that recorded in previous HALO measurements in the stratosphere, but was moderate in absolute terms; strong turbulence events remained rare. Turbulence intensity was higher in the eastern Atlantic (near Cape Verde) and closer to the equator, often associated with large convective systems. The relationship between the observed turbulent kinetic energy (TKE) and the energy dissipation rate ε matches the theoretical expectations $\varepsilon \propto \mathrm{TKE}^{3/2}$, allowing estimates of the outer scale of turbulence. There is a preliminary, weak indication that upper-tropospheric turbulence is indeed reduced above the doldrums. The relationship is not exclusive; low-level calms do not always guarantee reduced upper-level turbulence, and significant atmospheric variability exists. While the thermal stability in the upper troposphere above the doldrums is comparable to that of all circular flight legs, ECMWF's meteorological analyses indicate a reduction of vertical shear above the doldrums. This tentative link requires further investigation: High-resolution modeling or additional data are needed for robust conclusions.

https://doi.org/10.5194/egusphere-2026-2628
Preprint. Discussion started: 29 May 2026

1 Introduction

The Encyclopædia Britannica (https://www.britannica.com/science/doldrums) defines the doldrums as "equatorial regions of light ocean currents and winds located within the Intertropical Convergence Zone (ITCZ), a belt of *converging winds and rising air* that encircles the Earth near the equator"[1]. This traditional view was recently challenged by Windmiller (2024) who presented evidence of regions with low near-surface winds associated with *descending* airflow inside the Atlantic ITCZ. From this perspective, the doldrums represent a mesoscale component of the complex internal dynamics of the ITCZ (Windmiller and Stevens, 2024). It is therefore no surprise that these flow patterns had to be rediscovered in storm-resolving numerical simulations (Klocke et al., 2017), since they no longer pose a danger to powered shipping today, as they did in the days of sailboats.

Windmiller (2024), analyzing buoy data of 700 events, identified and proposed a mechanism on time scales of hours that contests the traditional view: the weak low-level winds throughout the doldrums are caused by areas of sinking air, compensating for the spatially smaller regions of convective updrafts, which, contrary to previously assumed convergence, create divergence at low altitudes (https://news.agu.org/press-release/new-explanation-doldrums-slow-wind/). The median duration of the doldrums, determined from the composite analysis of the buoy data, ranges from 20 minutes to approximately 9 hours. Overall, the doldrums are rare events (less than 5% of observation time) and usually occur between episodes of convective precipitation (Windmiller, 2024). Therefore, the doldrums characterize a mesoscale flow component of the ITCZ and they should not be confused with the horse latitudes, the calm regions of the subtropics associated with the subtropical ridge (Klocke et al., 2017). This high-pressure belt is caused by the dry, descending branch of the Hadley cell at $\sim 30°$[2]. Nonetheless, the doldrums, as equatorial calms, are considered as the light, rather unpredictable, and changeable winds within the ITCZ.

In this paper, extensive airborne observations during the 2024 PERCUSION ("Persistent EarthCARE underflight studies of the ITCZ and organized convection") campaign (https://orcestra-campaign.org/percusion.html) are used to investigate the following hypothesis:

- If descending air flows, are responsible for the calm near-surface winds of the doldrums, then the upper-level airflow should be affected as well. Essentially, the upper troposphere should become thermally stabilized due to the subsidence. Thermal stabilization in a column above the doldrums would lead to a reduction in turbulence. This hypothesis is being tested here by combining in-situ observations at flight level from the German research aircraft HALO with meteorological

[1]The 1911 edition of the Encyclopædia Britannica describes the doldrums as: "DOLDRUMS (a slang term, dol = dull; cf. tantrum), the region of calms near the equator where the trade-winds die away, a region of constant precipitation in which the weather is close, hot, vaporous and extremely dispiriting. In the old days of sailing vessels, a becalmed ship sometimes lay helpless for weeks. A letter from this region saying “we are in the doldrums” (“in the dumps”) seems to have been regarded as written from “The Doldrums,” which thus became the name of this undesirable locality." (https://en.wikisource.org/wiki/1911_Encyclop%C3%A6dia_Britannica/Doldrums)

[2]There is a curious discrepancy in the work of Windmiller: The poem "The rime of an ancient mariner" by S. T. Coldrige cited there speaks of ’days after days’ of calm. This period is significantly longer than the duration of episodes as detected by Windmiller (2024). Presumably, vessels caught in an equatorial calm might drift there for longer periods, contrary to the short time scales provided by the analysis of moored buoys. Another wonderfully compelling account of a long-lasting calm and its impact on human behavior onboard a sailboat trapped in the Gulf of Thailand was masterfully described by Joseph Conrad in his novel ’The Shadow Line’.

https://doi.org/10.5194/egusphere-2026-2628
Preprint. Discussion started: 29 May 2026

data from the ECMWF's Integrated Forecast System (IFS), which characterize the flow near the surface. The simple research question is therefore: Is the upper troposphere above the doldrums less turbulent?

- A second research question to be addressed in this article is: How much does the turbulence observed during PERCUSION (Groß et al., 2026; Stevens et al., 2026) in the tropical upper troposphere differ from measurements taken by the same airborne platform in the lower stratosphere during SOUTHTRAC (Rapp et al., 2021)?

Most of the knowledge about upper-level turbulence in tropical regions – which consists essentially of convectively-induced turbulence (CIT) or near-cloud turbulence (NCT) – comes from climatological analyses of turbulence reports from commercial aircraft (e.g. Sharman et al., 2012; Sharman and Lane, 2016; Sharman and Trier, 2019), from individual incidence reports (e.g. Gisinger et al., 2024; Wang, 2025), from individual case studies (e.g., Lane and Sharman, 2008; Trier et al., 2022), and from analyzing dedicated research flights (e.g., Kim et al., 2025; Atlas et al., 2025, 2026).

Kim et al. (2025) used measurements collected by a high-altitude research aircraft from NASA's "Dynamics and Chemistry of the Summer Stratosphere" (DCOTSS) field campaign to investigate atmospheric turbulence in the UTLS. This study focuses in particular on high flight altitudes (up to 7 km above the campaign-averaged tropopause of ∼14 km), which are never assessed by commercial aircraft and only occasionally by research aircraft (Kim et al., 2025, Fig. 1b). Typical observations of the eddy dissipation rate EDR (EDR $\equiv \varepsilon^{1/3}$, where ε is the energy dissipation rate) in the UTLS generally range from very low background EDR values below 0.05 $\mathrm{m}^{2/3}\,\mathrm{s}^{-1}$ up to about EDR $= 0.15\,\mathrm{m}^{2/3}\,\mathrm{s}^{-1}$, a value chosen as threshold for strong turbulence (Kim et al., 2025). The majority of observed EDR values are much lower with most measurements well below 0.05 $\mathrm{m}^{2/3}\,\mathrm{s}^{-1}$ and only about 0.34% of all measurements above 10 km altitude exceeded the strong turbulence threshold. Extremely strong turbulence (EDR $> 0.3\,\mathrm{m}^{2/3}\,\mathrm{s}^{-1}$) was rare and was mainly observed in moist plumes associated with deep convection within 2 km above the tropopause, corresponding to 1-2 km above the tops of deep convective clouds. Strong turbulence increases with proximity to convection, with elevated frequencies persisting up to a distance of 100 km from the convective core (Kim et al., 2025, Fig. 3c). These findings are consistent with findings from Atlas et al. (2026) and with observations of the LOON project (Köhler et al., 2023, Fig. 2).

The significance of small-scale turbulence for the local transport of trace gases and their injection into the tropical stratosphere as well as its dependence on the ambient atmospheric conditions was recently highlighted by Atlas et al. (2025). As in the study by Kim et al., they related the occurrence of enhanced turbulence to the modulation of the background flow in the tropical stratosphere through mesoscale dynamical processes. In particular, the fraction of the observed 200 m thick turbulent layers in the equatorial lower stratosphere varies over a factor of ten depending on the phase of the quasi-biennial oscillation (QBO). During QBO phase transitions, especially negative-to-positive transitions, Kelvin waves increase the local wind shear, reducing the Richardson number and promote turbulent instabilities. The decisive of the ambient atmospheric conditions (less shear) was confirmed by weaker observed turbulence when the QBO phase is well-established and during its negative phase (Atlas et al., 2025).

Jaffeux et al. (2025) derived ε for flights with the French SAFIRE-ATR42 during the MAESTRO campaign, another member of the ensemble during ORCESTRA (Stevens et al., 2026). These flights were conducted near Cape Verde in an area from 25°W

https://doi.org/10.5194/egusphere-2026-2628
Preprint. Discussion started: 29 May 2026

to 21°W and 13°N to 19°N and at three flight levels in the lowest and middle troposphere up to 6 km altitude (Jaffeux et al., 2025, Fig. 2). On seven days (MMDD in 2024: 0813, 0816, 0822, 0825, 0827, 0829, and 0903), coordinated flights were conducted with HALO during PERCUSION in the SAFIRE-ATR42 observational area (Jaffeux et al., 2025). Dissipation rates ε were estimated using Kolmogorov scaling in the inertial subrange. Overall, the SAFIRE-ATR42 observations show that ε is highest near the sea surface and decrease with increasing altitude; however, no $\varepsilon > 10^{-3}\,\mathrm{m^2\,s^{-3}}$ (EDR $\sim$ $0.1\,\mathrm{m^{2/3}\,s^{-1}}$) have been reported (Jaffeux et al., 2025, Fig. 17), which are surprisingly low values for the tropical troposphere.

Atlas and Bretherton (2023) analyzed NASA's WB-57 aircraft measurements of five tropical field campaigns to quantify the the variability of the vertical wind in the tropical tropopause layer (TTL), distinguishing between contributions from gravity waves (GWs) with short waveleghts (< 5 km) and long wavelengths (between 5 and 100 km) as well as turbulence. The paper shows evidence that short GWs and turbulence enhance thick, ice-rich cirrus clouds in the TTL. This study uses a threshold of $\varepsilon = 10^{-3}\,\mathrm{m^2\,s^{-3}}$ (EDR $= 0.1$ $\mathrm{m^{2/3}\,s^{-1}}$) to identify turbulence in the TTL (Atlas and Bretherton, 2023, Fig. B3). The distributions of EDR in the TTL, when categorized by ice water content, distance from deep convection, and altitude, generally show that most ε values are below $10^{-2}\,\mathrm{m^2\,s^{-3}}$ (EDR $\approx 0.215\,\mathrm{m^{2/3}\,s^{-1}}$), with the majority of ε in the turbulent patches falling between 10^{-4} and $10^{-2}\,\mathrm{m^2\,s^{-3}}$. Again, elevated EDR values are detected in about 1-2% of the TTL flight data, and turbulence rarely occurs in the absence of GW activity. The comparison between aircraft observations and numerical simulations of the small-scale variability of the vertical wind in the TTL reveals significant discrepancies: All four global storm-resolving models have too little resolved vertical wind at horizontal wavelengths between 10 and 100 km compared to aircraft observations indicating the small-scale GW activity is underrepresented in all the models due to the insufficient horizontal and vertical resolutions.

Comparison with the predictions of numerical model is one crucial aspect; another relevant point is the precise and comparable characterization of atmospheric turbulence with one highly accurate, well-calibrated measuring system. Here, the "Basic HALO Measurement and Sensor System" (BAHAMAS) from the German research aircraft HALO (Krautstrunk and Giez, 2012; Giez et al., 2017, 2019, 2022, 2025) is employed to quantify turbulence in the upper troposphere over the tropical Atlantic based on research flights conducted as part of EUREC^{4}A ("Elucidation of the Role of Cloud-Circulation Interactions in Climate", Stevens et al., 2021) as well as the PERCUSION campaign ("Persistent EarthCARE underflight studies of the ITCZ and organized convection", Stevens et al., 2026).

Previously, measurements by BAHAMAS were used to investigate the horizontal spectrum of vertical velocities from various aircraft campaigns (Schumann, 2019) and particular turbulence incidents encountered by HALO (e.g., Bramberger et al., 2020; Wilms et al., 2020; Woiwode et al., 2023; Rodriguez Imazio et al., 2022, 2023). Dörnbrack et al. (2022) used the BAHAMAS measurements from the whole field campaign SOUTHTRAC to investigate the turbulence in the upper troposphere, lower stratosphere (UTLS) and to compare the observations with the IFS's operational turbulence forecasts, which were recently put into operation (Bechtold et al., 2021a, b; Ko et al., 2025). Of course, research flights are not deliberately conducted in regions where severe turbulence is expected. If such areas are encountered, it is a mere coincidence and the flight is aborted, as the Iceland case has shown (Bramberger et al., 2020).

https://doi.org/10.5194/egusphere-2026-2628
Preprint. Discussion started: 29 May 2026

What's more, research flights are temporary, highly localized endeavors, and their results can only provide snapshots of atmospheric conditions where aircraft can safely operate. Such measurements cannot claim to investigate extreme events or to establish a comprehensive global climatology of atmospheric turbulence. Nevertheless, it is a fascinating question what the turbulent state of the atmosphere looks like when data from research flights are evaluated, whose flight patterns were planned and flown for completely different reasons. Another aspect, which has already been touched on in the preceding paragraphs, is the question of how far CIT can extend from the actual convective storms (Sharman and Trier, 2019). Hitchcock et al. (2025) reported about earlier studies suggesting that CIT of moderate-or-greater (MoG) intensity may extend beyond the current avoidance guidelines for airliners (20 miles or 32 km). They emphasize that many questions remain unanswered regarding the spatial distribution of turbulence in relation to convective storms and the influence of ambient atmospheric conditions on turbulence intensity.

The paper is organized in six sections. Section 2 introduced the observational data and the methodology to analyze them. Section 3 compares a selected dataset of 10- and 100-Hz BAHAMAS wind data from EUREC^{4}A to establish confidence in the EDR results of the only available 10-Hz data, which are used to analyze the turbulence during PERCUSION in the following section 4. Section 5 answers the first research question formulated above and Section 6 concludes the paper.

2 Methodology

2.1 Observational Data

Airborne in-situ data from the Basic HALO Measurement and Sensor System (BAHAMAS) on board the German research aircraft HALO (Krautstrunk and Giez, 2012) are analyzed to investigate turbulence at flight level. An important part of BAHAMAS is a nose boom-mounted precision air flow sensor. The data from this 5-hole probe is used to determine in situ measurements of the horizontal and vertical wind components u, v, and w. The measurement system additionally provides temperatures, pressures, and water vapor mixing ratios with high temporal resolution, i.e. up to 100 Hz (Giez et al., 2017, 2019). Giez et al. (2021, 2022) presented a detailed and complete description of the different calibration steps of the BAHAMAS sensor for HALO. BAHAMAS data are distributed with a temporal resolution of 1 and 10 Hz by default. BAHAMAS data with a high temporal resolution of 100 Hz are only available after special post-processing for selected limited periods of HALO field campaigns. For example, Appendix B of Dörnbrack et al. (2022) demonstrates that the spectra of the 10 and 100 Hz data within the analysis interval of 0.4 to 4 Hz, which is used to determine the energy dissipation rates ε, are very similar, a result that enhances confidence in the well-calibrated BAHAMAS measurements Giez et al. (2021). According to Giez et al. (2025), the absolute errors (1σ) of the aircraft-relative horizontal and vertical wind components u_b, v_b, and w are 0.3 m s^{-1}, 0.5 m s^{-1}, and 0.6 m s^{-1}, respectively.

Turbulence measurements are currently not possible during climb and descent, especially when aerodynamic aids (spoilers, flaps, etc.) are used. To date, no data from in-flight calibration of the flow probe is available for these flight conditions/aircraft configurations. Strictly speaking, turbulence data can only be processed with an aircraft in stable, straight and constant altitude flight, as the calibration parameters used for the flow probe were only determined under these conditions (Giez et al., 2017).

https://doi.org/10.5194/egusphere-2026-2628
Preprint. Discussion started: 29 May 2026

Nevertheless, the analysis of turbulence data by Giez et al. (2025) has shown that the high-frequency wind data is apparently not affected by aircraft turns. Roll angle and heading do not impact the wind measurements. For these reasons, BAHAMAS data is generally made available for aircraft turns as well. The only exceptions are particularly steep curves or very abrupt/rapid turning maneuvers.

In this study, BAHAMAS measurements of the three wind components u, v, and w are analyzed at constant altitude for the two tropical airborne campaigns EUREC^{4}A(Stevens et al., 2021) and PERCUSION (Groß et al., 2026; Stevens et al., 2026). For EUREC^{4}A, ten flight legs are selected where both 10 and 100 Hz BAHAMAS data are available. The comparison of these two data sets should further strengthen confidence in the analysis of the 10 Hz data that are available for the PERCUSION campaign. For this campaign, 23 research flights over the tropical Atlantic were analyzed.

2.2 Determination of TKE and the energy dissipation rate ε

The specific turbulent kinetic energy TKE and energy dissipation rates ε_i (i stands for the velocity components u, v, w, respectively) are calculated from the BAHAMAS data along all constant level HALO flight legs. Each flight leg is divided into 16 s segments, each 4 s apart for which the perturbations of the velocity components u', v', and w' are determined by subtracting second-order polynomial fits. These perturbations u', v', and w' are used to compute the specific turbulent kinetic energy TKE

$$\mathrm{TKE} = \frac{1}{2}\left(\overline{u'^2} + \overline{v'^2} + \overline{w'^2}\right), \tag{1}$$

where the overbar represents the mean over the 16 s segments. Based on the experiences of Dörnbrack et al. (2022), this study only investigate the energy dissipation rate ε_w derived from the inertial subrange technique

$$S_w(k) = \alpha_w \varepsilon_w^{2/3} k^{-5/3}, \quad \text{i.e.,} \quad \varepsilon_w = \left(\frac{S_w\, k^{5/3}}{\alpha_w}\right)^{\frac{3}{2}} \tag{2}$$

where k is the wavenumber and $\alpha_w = 0.707$ is the Kolmogorov constants for w (Oncley et al., 1996; Piper and Lundquist, 2004; Strauss et al., 2015). The spectral energy density S_w is computed in the 16 s segments applying the Welch method for the partially overlapping segments and a Tukey filter to mitigate the effects of jumps due to the aperiodicity of the data (Sharman et al., 2014, Sec. 2c). It must be noted that the spectra are computed in the frequency domain and then transformed into the wavenumber space employing $k = f/V_{\mathrm{TAS}}$, where V_{TAS} is the mean true-airspeed of HALO in the 16 s segments. A thorough overview of different methods to estimate ε from aircraft measurements is provided by Wacławczyk et al. (2020).

To ensure comparability with published results from HALO measurements, the identical frequency window from 0.4 to 4 Hz is utilized in our investigation. The limits of 0.4 and 4 Hz are deliberately selected to avoid, on the one hand, peaks caused by the oscillations of the nose boom and, on the other hand, the noise of the data, i.e. V_{TAS} for u_{b}, side slip angle β for v_{b} (u_{b} and v_{b} are the longitudinal/lateral horizontal velocity components with respect to the aircraft) and the angle of attack α for w, as far as possible; see discussions in Appendix A of Giez et al. (2025) or Appendix B of Dörnbrack et al. (2022).

In this way, the spectrum represents the average over 16 s or $\sim$4 km flight distance and resolves motion scales down to 4 Hz or $\sim$ 60 m horizontal distance. The determination of TKE in exactly the same segments where ε_w was estimated allows to test

https://doi.org/10.5194/egusphere-2026-2628
Preprint. Discussion started: 29 May 2026

the theoretical dependence

$$\varepsilon = C_\varepsilon \frac{TKE^{3/2}}{\ell}, \tag{3}$$

where ℓ is a characteristic integral length scale of the large turbulent eddies (Vassilicos, 2015; Wacławczyk et al., 2020, 2025). Equation 3 essentially states that a normalized dissipation rate C_ε is constant across a certain wavenumber (frequency) range of the turbulent spectrum. Vassilicos (2015) states that Eq. 3 with $C_\varepsilon = \text{const.}$ is a cornerstone assumption on which the Kolmogorov-Richardson cascade rests, see also Tennekes and Lumley (1972). Recently, Vassilicos (2015) has shown that C_ε is not constant because it is influenced by the details of the turbulent flow's large-scale structure, the nature of its forcing, or the initial conditions, and whether the turbulence is forced or decaying. These dependencies lead to significant variability in C_ε across different flows and conditions, challenging the universality assumed in classical turbulence theory, see Wacławczyk et al. (2025).

The two quantities TKE and ε_w, determined from the aircraft measurements, have slightly different meanings. While ε_w represents the rate of energy transported downscale in the energy cascade, TKE is a measure of the total intensity of turbulent eddies in the segments under consideration. TKE is the half sum of all the velocity variances both in physical and spectral space. In contrast, ε_w is proportional to S_w only in the selected and limited frequency (wavenumber) range and its estimate assumes a $k^{-5/3}$ spectral slope, Eq. 2.

Besides the integral length scale ℓ as introduced in Eq. 3, there are two fundamental length scales for stratified turbulence. The Kolmogorov microscale

$$\eta = \left(\frac{\nu^3}{\varepsilon}\right)^{1/4} \tag{4}$$

is the inner scale of velocity fluctuations where kinetic energy is viscously dissipated into heat (Kolmogorov, 1941). Here, the kinematic viscosity $\nu = \mu/\rho$ can be calculated from the temperature dependent dynamic viscosity μ using the Sutherland formula (White, 1991, Eq.1-36) and the air density ρ. The Ozmidov scale

$$\mathrm{L_O} = \left(\frac{\varepsilon}{\mathrm{N}^3}\right)^{1/2} \tag{5}$$

is smallest scale for which buoyancy effects are important (e.g., Khani and Waite, 2014). In other words, L_O is the largest scale where the flow resembles a three-dimensional isotropic turbulence, see Ozmidov (1965) or (Riley and Lindborg, 2008, Appendix A). Here, the buoyancy frequency

$$N = \sqrt{\frac{g}{\Theta}\frac{\partial \Theta}{\partial z}}, \tag{6}$$

can be calculated from the vertical distribution of the potential temperature Θ, g the gravitational acceleration. As this distribution is not available from the airborne measurements, data from a numerical weather prediction (NWP) model interpolated on HALO's flight tracks are used instead, see next Section 2.3.

In addition, as we investigate turbulence in a stably stratified atmosphere, vertical velocity fluctuations are suppressed by buoyancy leading to an anisotropic flow with flat horizontal motions. The thickness of the resulting layers is given by

$$L_B = \frac{u_{rms}}{N}, \tag{7}$$

https://doi.org/10.5194/egusphere-2026-2628
Preprint. Discussion started: 29 May 2026

where u_{rms} is a typical turbulent velocity. This length scale is also called the buoyancy scale.

2.3 ECMWF IFS

The Integrated Forecast System (IFS) is the state-of-the-art global numerical weather prediction (NWP) system operational at the European Centre for Medium-Range Weather Forecasts (ECMWF). To establish a relation between the in situ observations and the ambient atmospheric conditions, 1-hourly analyses of the ERA5 data (Hersbach et al., 2020) are used to compute the vertical shear $S = \sqrt{\left(\frac{\partial U}{\partial z}\right)^2 + \left(\frac{\partial V}{\partial z}\right)^2}$, the buoyancy frequency N, and the Richardson Number $Ri = N^2/S^2$ along the HALO flight legs for the PERCUSION campaign. Here, U and V denote the zonal and meridional wind components. In addition, the temperature data along HALOs legs are used to determine the local height of the cold-point tropopause (e.g. Kim and Son, 2012; Tegtmeier et al., 2020, CPT).

In addition, the following 2D fields are used to describe the atmospheric conditions under which the PERCUSION flights were conducted. There is the magnitude of the horizontal wind at 10 m altitude $|u_{10\,\mathrm{m}}| = \sqrt{u_{10\,\mathrm{m}}^2 + v_{10\,\mathrm{m}}^2}$. This quantity is used to specify the near-surface flow underneath the HALO legs. There is total column water (TCW), i.e. the sum of water vapor, liquid water, cloud ice, rain and snow in a column extending from the surface of the Earth to the top of the atmosphere. This quantity was used as a means to determine location of the ITCZ. A threshold of $48\,\mathrm{kg\,m^{-2}}$ is applied here, i.e. HALO positions with TCW $> 48\,\mathrm{kg\,m^{-2}}$ are considered to be within the ITCZ. Finally, the total column vertically-integrated divergence of mass flux (VIMAD in $\mathrm{kg\,s{-}1\,m^2}$) is used to specify convergence and divergence. VIMAD is the horizontal rate of flow of mass across the flow for a column of air extending from the surface of the Earth to the top of the atmosphere. This parameter is positive for mass that is spreading out, or diverging, and negative for the opposite, for mass that is concentrating, or converging (convergence). This parameter thus indicates whether atmospheric motions act to decrease (for divergence) or increase (for convergence) the vertical integral of mass. In the analysis of Section 5, it is implicitly assumed that most of the mass of the atmosphere is confined to the lower troposphere and VIMAD represents mainly this part of mass flux.

Generally, the ERA5 data are available at 137 hybrid model levels from the surface to ~ 80 km altitude and provide hourly estimates of atmospheric variables at a horizontal resolution of ~ 30 km. All the IFS data are interpolated on HALO's flight legs in space and time and, in the case of the circular legs flown during PERCUSION, on squares enclosing the respective circles.

2.4 Rain Rate

To quantify the spatial and temporal distribution of convective thunderstorms, the re-processed and bias-corrected 30-minute CMORPH precipitation rate data product is used (Xie et al., 2017). CMORPH is provided on a latitude and longitude grid with a resolution of $0.0727° \times 0.0727°$, equivalent to a resolution of 8 km at the equator (Xie et al., 2019). Recently, Stephan and Stevens (2025) used CMORPH as the primary observational reference dataset to validate the precipitation cluster statistics of global high-resolution numerical simulations. Their analysis confirms that the scaling behavior of the model precipitation agrees well with the fractal dimensions derived from CMORPH. Therefore, CMORPH is well-suited for representing the actual storm activity over the tropical Atlantic during PERCUSION.

https://doi.org/10.5194/egusphere-2026-2628
Preprint. Discussion started: 29 May 2026

3 EUREC^{4}A

High-resolution 100 Hz BAHAMAS data over the tropical Atlantic are available from the EUREC^{4}A mission (e.g., Stevens et al., 2021). The HALO research flights were conducted from Barbados and investigated shallow convection in the prevailing trade wind weather regime from late January to early February 2020. Table 1 lists the available 12 flight legs with 100 Hz BAHAMAS data, amounting to a total of 31220 s ($\sim$ 8.7 h) of data from flights in the troposphere at two different altitudes. All analyzed flights took place between 10.1°N and 14.6°N and from 59°W and 51°W. In addition, the 10 Hz BAHAMAS data were analyzed for the same HALO legs. The comparison of the 100 Hz and 10 Hz data shall give confidence in using the 10 Hz data which are only available for the PERCUSION mission.

Track Name	Begin (UTC)	End (UTC)	Duration (s)	Height (km)
0128_T1	18:30:00	19:02:00	1920	10.3
0128_T2	19:06:00	20:00:00	3240	10.3
0130_T1	11:34:00	12:34:00	3600	10.3
0130_T2	12:38:00	13:55:00	4600	10.3
0130_T3	13:57:00	14:42:00	2700	10.3
0213_T1	11:33:00	12:07:00	2040	10.3
0213_T2	12:15:00	12:58:00	2580	10.3
0215_T1	17:30:00	17:48:00	1080	5.8
0215_T2	18:02:40	18:09:10	420	5.8
0215_T3	18:11:00	18:19:40	480	5.8
0215_T4	18:34:20	19:35:00	3600	5.8
0215_T5	19:36:00	21:00:00	5040	5.8

Table 1. HALO flight tracks during EUREC^{4}A for which 100 Hz BAHAMAS data are available. The flights were conducted from Barbados in January and February 2020.

Figure 1 depicts the power spectra of the vertical wind component S_w for the 10 longest HALO flight legs as function of frequency f and wavenumber k. There are legs with larger spectral energy density S_w, e.g. the legs 0215_T5, 0128_T2, and 0130_T2. However, these few spectra alone do not provide sufficient evidence to conclude that S_w increases or decreases with altitude. The 100 Hz data follow a slope of approximately $k^{-5/3}$ in a frequency (wavelength) range $f > 1$ Hz ($\lambda \lesssim 100$ m, panels (a) and (b) in Fig. 1). The S_w spectra of the 10 Hz data, although showing the same magnitudes, have flatter slopes,

https://doi.org/10.5194/egusphere-2026-2628
Preprint. Discussion started: 29 May 2026

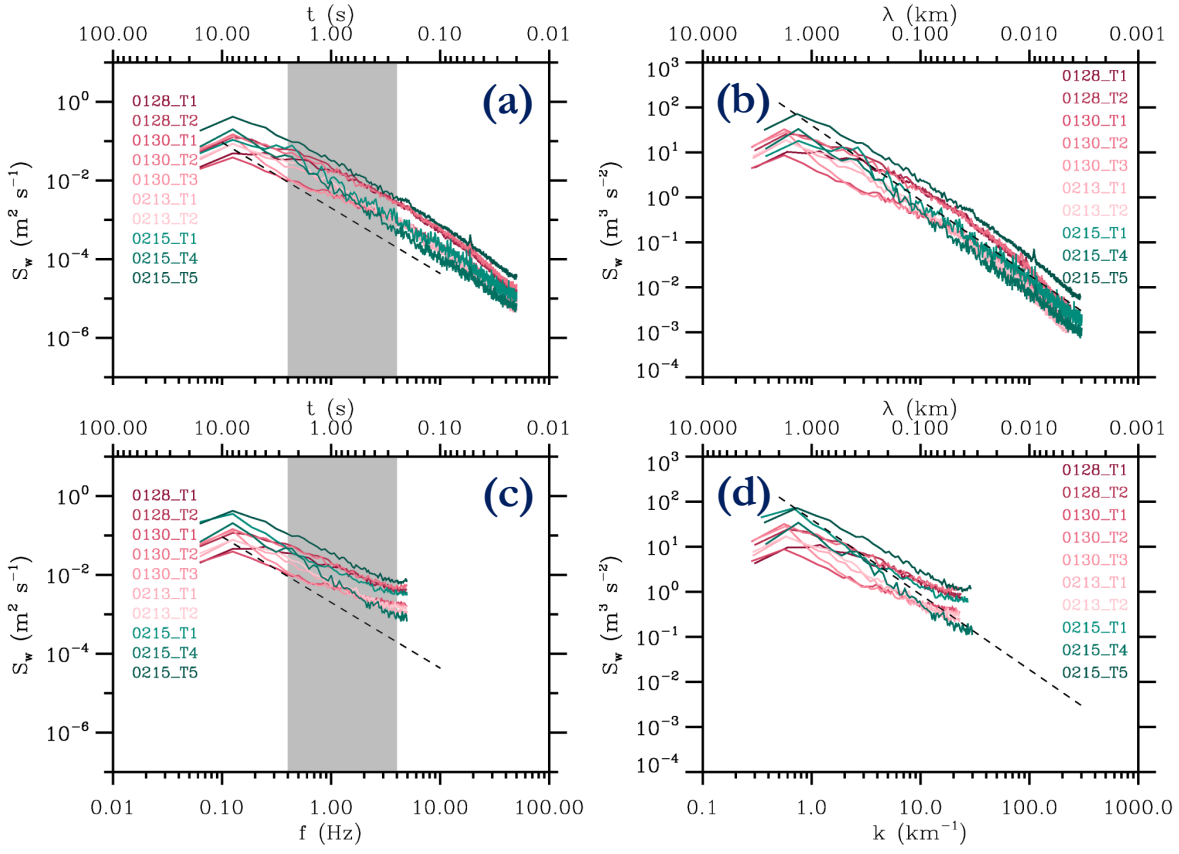

Figure 1. Power spectra of the vertical velocity w as function of frequency f (a, c) and wavenumber k (b, d) for the HALO's legs where 100 Hz BAHAMAS data are available during EUREC^{4}A. The different colors mark the month and day of 2020 and the corresponding labels of each flight leg with the greenish lines representing the lower HALO flight levels (Table 1) and the dashed lines show the $f^{-5/3}$ or $k^{-5/3}$ slopes. (a, b): 100 Hz BAHAMAS data, (c, d): 10 Hz BAHAMAS data. The gray segments in (a) and (c) indicate the frequency range for which EDR_w is estimated.

panels (c) and (d) in Fig. 1. The frequency range highlighted in gray indicates the range for which EDR_w is determined using the method described in Sec. 2.2.

Panels (a) and (b) of Figure 2 provide an impression of the spatial distribution of the EDR_w values as a function of geographical longitude. EDR_w varies between small values less than 0.05 $m^{2/3}\,s^{-1}$ and a peaks exceeding 0.15 $m^{2/3}\,s^{-1}$. As expected from the spectra in Fig. 1, the largest EDR_w values occur for the HALO tracks 0215_T5 and 0130_T2. Despite minor differences in individual peak values, the EDR_w values derived from the 100 Hz and 10 Hz BAHAMAS data match in terms of their spatial distribution and overall magnitude. The calculated TKE distributions for both data sets, as shown in panels (b) and (d) of Fig. 2, confirm the EDR_w results regarding the intermittent occurrence of turbulence and the overall agreement between

https://doi.org/10.5194/egusphere-2026-2628
Preprint. Discussion started: 29 May 2026

the data at 10 Hz and 100 Hz. As described in Section 2.2, TKE is calculated for exactly the same segments in which the spectra are calculated. Therefore, its spatial distribution resembles that of EDR_w, with differences in the magnitude and width of the turbulence events, which could be caused by horizontal wind disturbances u' and v' and the broader frequency (wave number) range for which the TKE is calculated.

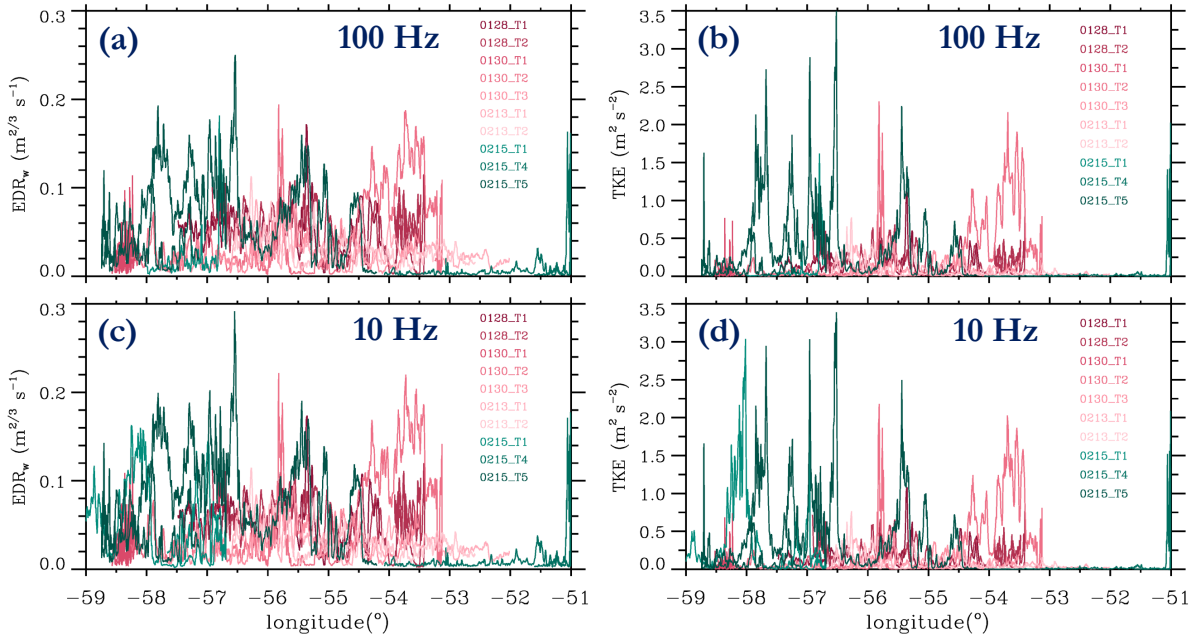

Figure 2. EDR_w (a, c) and TKE (b, d) as function of longitude along the HALO's legs where 100 Hz BAHAMAS data are available during EUREC^{4}A. The different colors mark the month and day of 2020 and the corresponding labels of the individual flight legs, with the greenish lines representing the lower HALO flight levels, see Table 1. (a, b): 100 Hz BAHAMAS data, (c, d): 10 Hz BAHAMAS data.

Figure 3 compares the probability density distributions of ε_w from two measurement campaigns on the one hand – SOUTHTRAC serves as an example of BAHAMAS observations in the lower stratosphere that have been fully analyzed and published (Dörnbrack et al., 2022) – and from the 100 Hz and 10 Hz data for EUREC^{4}A on the other. First of all, the measurements from the EUREC^{4}A project show a larger relative number of higher ε_w values than those measured during SOUTHTRAC. For example, during SOUTHTRAC the relative portions of the estimated ε_w with values larger than 10^{-5}, 10^{-4}, $10^{-3}\,\mathrm{m^2\,s^{-3}}$ amount to of 12.3%, 4.1%, and 0.7%, respectively. For EUREC^{4}A, the corresponding numbers for the 100 Hz (10 Hz) BAHAMAS data are: 56% (64%), 28% (33%), and 5.7% (8.2%), respectively. Although the EDR_w values do not indicate MoG turbulence ($\mathrm{EDR}_w > 0.18\,\mathrm{m^{2/3}\,s^{-1}}$), the general increase of turbulence intensity is plausible, as the flights during EUREC^{4}A always took place in the turbulence-prone tropical troposphere, whereas the SOUTHTRAC flights were conducted primarily in the lower stratosphere, see Figures 1 and 2a of Dörnbrack et al. (2022). In both campaigns, computed EDR_w values with peaks greater than $0.18\,\mathrm{m^{2/3}\,s^{-1}}$ ($\varepsilon_w \gtrsim 6{\cdot}10^{-3}\,\mathrm{m^2\,s^{-3}}$) occur very rarely, Figure 2a and c. Moreover, by comparing the blue curves

https://doi.org/10.5194/egusphere-2026-2628
Preprint. Discussion started: 29 May 2026

in Fig. 3, it is evident that there are only minor differences in the corresponding distributions of the 10 and 100 Hz BAHAMAS data for the EUREC^{4}A campaign.

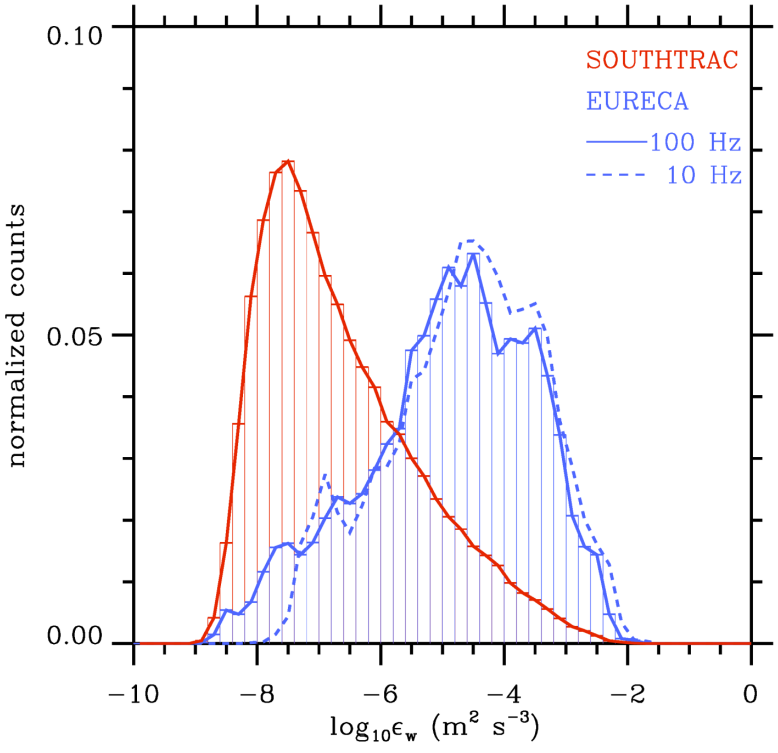

Figure 3. Probability density distributions of ε_w for the HALO's legs where 100 Hz BAHAMAS data are available during EUREC^{4}A (blue lines) and for the SOUTHTRAC 10 Hz (red lines) data as published in Dörnbrack et al. (2022).

Figure 4 shows TKE as function of ε_w in a log-log representation. The slopes indicted in both panels are computed assuming that neither TKE nor ε_w are truly independent variables, so the bisecting lines of TKE vs ε_w and ε_w vs TKE are calculated (robust regression). A pure linear regression would result in the following slope values for the 10 (100) Hz data: 0.52 (0.47), 0.64 (0.63), 0.67 (0.68), and 0.68 (0.64) for the different ε_w ranges indicated in Fig. 4. In comparison to the slopes listed in Fig. 4, these values are close to 2/3 and don't increase for intervals at higher ε_w. The comparison of the 100 Hz and 10 Hz BAHAMAS data demonstrate that the 10 Hz data can be reliably used to characterize turbulence using the spectrally determined energy dissipation rate ε_w and the TKE. Both the slopes of the 100 and 10 Hz BAHAMAS data show very similar values, which reinforces confidence in the 10 Hz data for characterizing atmospheric turbulence from the HALO measurements.

From a physical point of view, it is encouraging and reassuring to see that the calculated slope values are reasonably close to the expected value of 2/3, which is derived from Eq. 3. In particular, both the robust and the linear regressions for $\varepsilon_w > 10^{-5}$ m^2 s^{-3} (green lines in Fig. 4) show that the calculated slopes are very close to 2/3. However, the robust regression

https://doi.org/10.5194/egusphere-2026-2628
Preprint. Discussion started: 29 May 2026

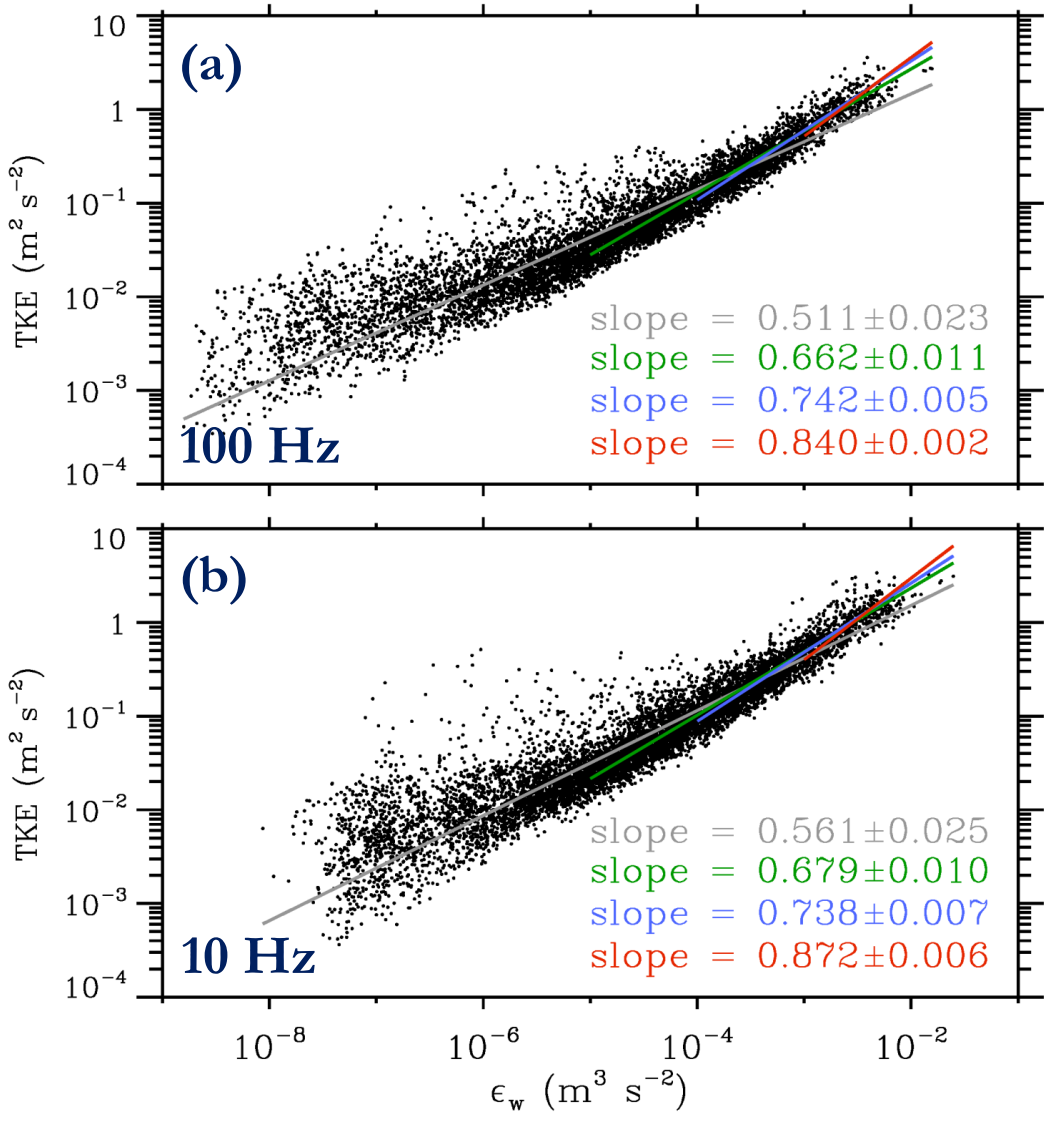

Figure 4. TKE as function of ε_w for all analyzed segments of the EUREC^{4}A research flights, (a): 100 Hz BAHAMAS data, (b): 10 Hz BAHAMAS data. The colored slope values refer to the linear regressions of $\log_{10}(\text{TKE}) = \text{f}(\log_{10}(\varepsilon_w))$ in the ε_w ranges indicated by the lengths of the respective lines, i.e., gray for $\varepsilon_w \geq 10^{-8}\,\text{m}^2\,\text{s}^{-3}$, green for $\varepsilon_w \geq 10^{-5}\,\text{m}^2\,\text{s}^{-3}$, blue for $\varepsilon_w \geq 10^{-4}\,\text{m}^2\,\text{s}^{-3}$, and red for $\varepsilon_w \geq 10^{-2}\,\text{m}^2\,\text{s}^{-3}$, respectively.

shows an increase by $\sim$25% when the ε_w range is restricted to stronger turbulence, i.e. to all values with $\varepsilon_w \geq 10^{-2}\,\text{m}^2\,\text{s}^{-3}$ (EDR $\gtrsim 0.215\,\text{m}^{2/3}\,\text{s}^{-1}$). Thus, a limited but long enough range excluding all small $\varepsilon_w < 10^{-5}\,\text{m}^2\,\text{s}^{-3}$ values is necessary in order to establish a robust relation between TKE and ε_w. From the regressions shown in Fig. 4, $\ell/C_\varepsilon \approx 348$ (288) m (for linear regression) was determined for $\varepsilon_w > 10^{-5}\,\text{m}^2\,\text{s}^{-3}$ (green lines in Fig. 4). Assuming C_ε lying between 0.5 and 2 depending on

https://doi.org/10.5194/egusphere-2026-2628
Preprint. Discussion started: 29 May 2026

the Reynolds number (Wacławczyk et al., 2025), the integral length scale ℓ ranges from about ~ 175 to ~ 770 m for the robust regression and from ~ 144 to ~ 475 m for the linear regression. A discussion of these values follows in Section 4.2.

4 PERCUSION

4.1 Overview

The PERCUSION campaign (Persistent EarthCARE underflight studies of the ITCZ and organized convection, Groß et al., 2026, https://orcestra-campaign.org/percusion.html) is a member of the research network ORCESTRA (Organized Convection and EarthCARE Studies over the Tropical Atlantic, Stevens et al., 2026). The HALO research flights during PERCUSION took place over Europe and over the tropical Atlantic. Here, we focus on the tropical part of the HALO research flights that were conducted from Cape Verde and Barbados in two periods of August to September 2024. As in former airborne campaigns (e.g. Stevens et al., 2019, 2021), HALO was equipped as a flying cloud observatory combining active and passive remote sensors (Groß et al., 2026, Table 3). Here, the BAHAMAS measurements mentioned above (section 2.1) are examined exclusively.

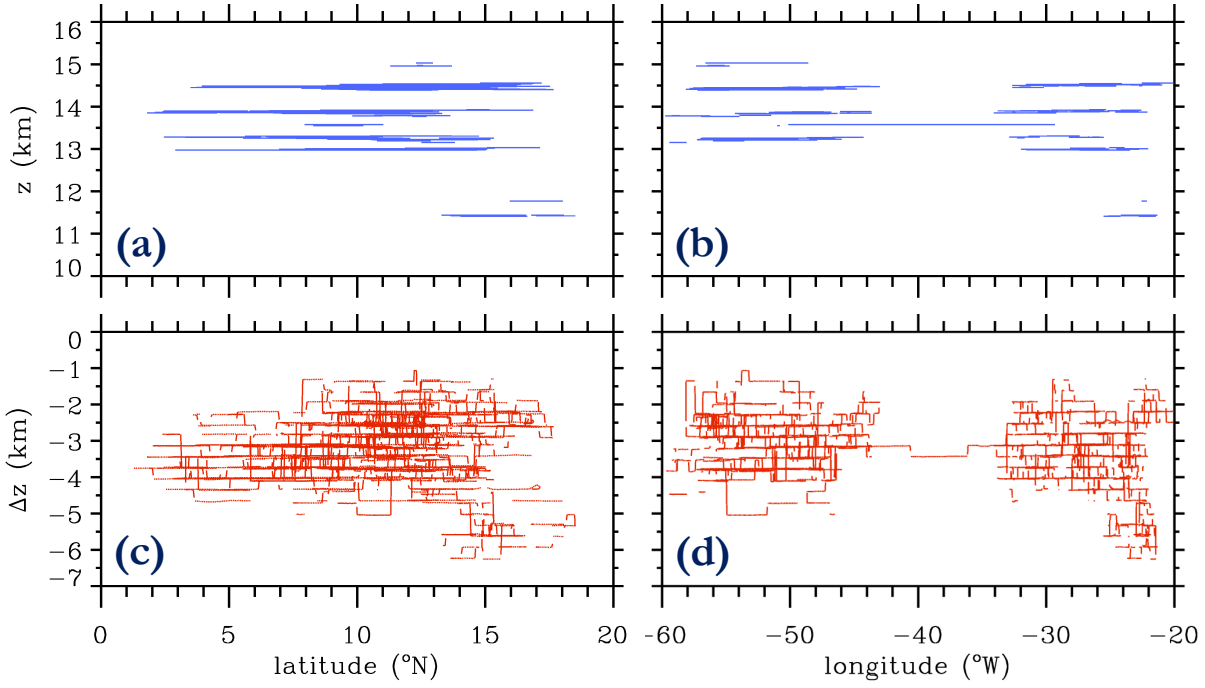

Figure 5. HALO's flight levels of the 183 constant altitude legs as function of latitude (a) and longitude (b). Panels (c) and (d) show the difference Δz of HALO's GPS altitude and the height of the local cold-point tropopause (CPT).

https://doi.org/10.5194/egusphere-2026-2628
Preprint. Discussion started: 29 May 2026

There were a total of 23 HALO flights stretching across tropical latitudes from the equator to $\sim 20°$N and from 60°W to 20°W. From all these research flights, 183 legs were identified during which HALO flew at a constant altitude. The individual flights were a combination of straight (mostly north-south oriented) legs and large (diameter ~ 200 km) and small (diameter less than 100 km) circles (Groß et al., 2026, Fig. 1). Most of these constant altitude legs were at altitudes between 13 and 15 km (Figure 5a and b). Despite the high flight levels, all flight legs were within the tropical troposphere, as the vertical distance Δz between the HALO GPS altitude and the local CPT only has negative values between -1 km and approximately -6 km (Figure 5c and d). According to Fig. 6e of Tegtmeier et al. (2020), the CPT altitudes derived from ERA5 differ by ~ -150 m from the radio occultation upper-air measurements, a result that does not affect the finding that all HALO flights during PERCUSION were in the upper troposphere. Furthermore, a recent study reveals that ERA5 reproduces the CPT height with good accuracy (deviations less than 500 m) when compared with both observations and global storm-resolving simulations (Nugent et al., 2025).

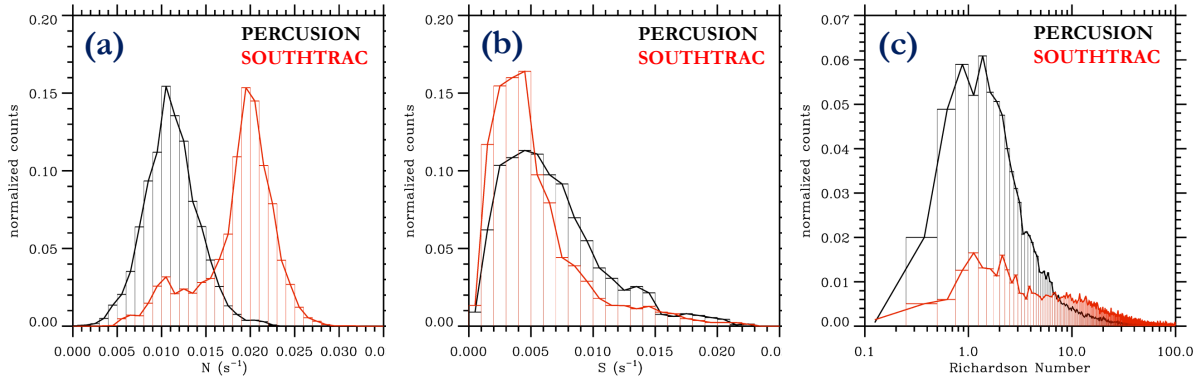

Figure 6. Computed probability density functions of the buoyancy frequency N (a), the vertical shear S (b) and the Richardson number (c) along HALO's constant altitude flight legs during PERCUSION (black) and SOUTHTRAC (red). The vertical lines represent the data binned according to the width of the bars, and the black curves connect the values in the middle of the bars.

.

To characterize the atmospheric background conditions, N, S and Ri interpolated on the 183 flight legs were computed from the IFS data (Section 2.3). Figure 6 presents the corresponding probability density distributions both for the PERCUSION flights as well as for the SOUTHTRAC flights as published in Dörnbrack et al. (2022). The difference in the thermal stratification N is obvious: the PERCUSION flights were conducted under conditions typical for the troposphere with the majority of observations centered at $N \approx 0.01\,\mathrm{s}^{-1}$ whereas the SOUTHTRAC flights show a clear dominance of the more stable stratification of the stratosphere centered at $N \approx 0.02\,\mathrm{s}^{-1}$, Fig. 6a. Approximately 90% (34%) of all PERCUSION flights exhibited values of $N < 0.015$ (0.01) s^{-1}, which stands in clear contrast to the correspondingly lower values of 19% and 6% during the SOUTHTRAC mission.

https://doi.org/10.5194/egusphere-2026-2628
Preprint. Discussion started: 29 May 2026

The shear distributions in Fig. 6b have single peaks at $S \sim 6.7 \cdot 10^{-3}\,\mathrm{s}^{-1}$, larger shear values $S > 10^{-2}\,\mathrm{s}^{-1}$ are relatively rare and amount to $\sim 18\%$ for the PERCUSION flights (for SOUTHTRAC the ratio is $\sim 10\%$). Therefore, the distribution of the vertical shear S for PERCUSION is broader compared to SOUTHTRAC, Fig. 6b. For both campaigns, there are $\sim 75\%$ of the data falling into the range $10^{-3}\,\mathrm{s}^{-1} \leq S \leq 10^{-2}\,\mathrm{s}^{-1}$. Consequently, the local Richardson numbers are predominantly larger than 1 (87% for PERCUSION, 96% for SOUTHTRAC), yet there are a few cases where the $\mathrm{Ri} < 0.25$ (about 0.6% for SOUTHTRAC and 2.1% for PERUSION), see Fig. 6c. Overall, the local atmospheric conditions in the upper troposphere during the PERCUSION research flights were dominated by an airflow under thermally stable conditions with low vertical shear and large Richardson numbers.

4.2 Upper-level Turbulence

Figure 7 shows the mean power spectra S_w of the 23 HALO flights during PERCUSION, with the respective mean value calculated as the average over all legs at constant altitude of one flight. The S_w magnitude varies by two orders of magnitude: The largest spectral amplitudes occur for the flights from Cape Verde (greenish lines), the lowest for the flights from Barbados (reddish lines). The spectral slopes largely follow the $-5/3$ law of the inertial subrange, but, as already shown for EUREC^{4}A in Fig. 1, all spectra flatten out at higher frequencies (wave numbers).

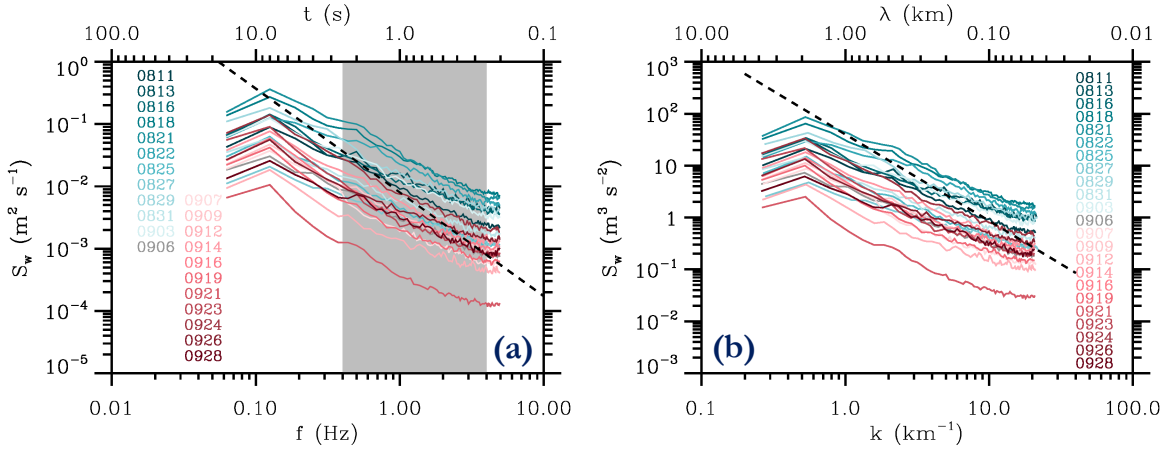

Figure 7. Mean power spectra S_w as function of frequency f (a) and wavenumber k (b) for the 23 research flights during PERCUSION. The different colors indicate the month and day of the year 2024 for each flight. The greenish lines represent the HALO flights from Cape Verde, the reddish lines those from Barbados, and the dashed lines show the slopes $f^{-5/3}$ or $k^{-5/3}$. The gray segment in panel (a) indicates the frequency range for which $\mathrm{EDR_w}$ is estimated.

Figure 8 illustrates the geographical distribution of the observed turbulence based on the TKE and the EDR_w, which were calculated as described in Section 2.2. There is a clear difference in turbulence intensity between flights in the eastern (greenish lines) and western (reddish lines) parts of the Atlantic: In the eastern part, EDR_w often reaches values of more than

https://doi.org/10.5194/egusphere-2026-2628
Preprint. Discussion started: 29 May 2026

0.3 $m^{2/3}\,s^{-1}$, see Fig. 8a. Moreover, these higher values occur closer to the equator than those observed over the western Atlantic, see Fig. 8b. The EDR_w values for these HALO flights from Barbados are similar to those measured during EUREC^{4}A, see Fig. 2c. The higher turbulence intensity of the measurements over the eastern Atlantic is also reflected in the TKE values, see Fig. 8c and d. Here, TKE values of up to 8 $m^2\,s^{-2}$ were measured on these flights from the Cape Verdes.

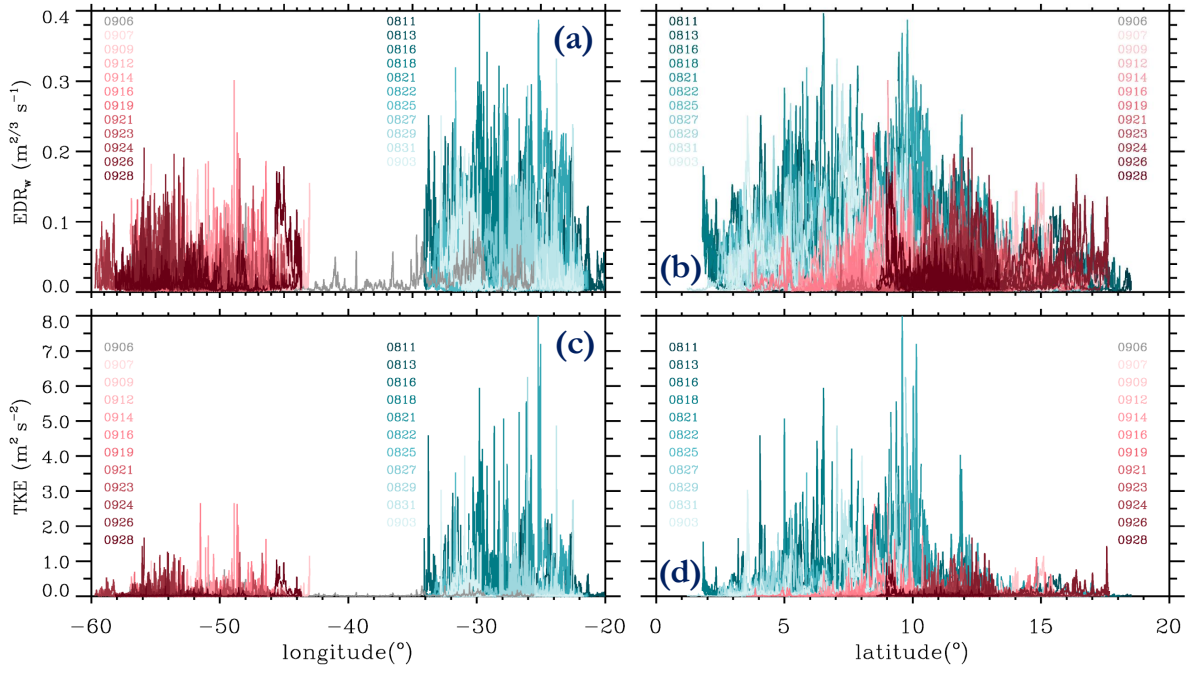

Figure 8. EDR$_w$ (a, b) and TKE (c, d) as function of longitude and latitude along 183 constant altitude legs of the 23 HALO flights during PERCUSION. The different colors indicate the month and day of the year 2024 for each flight. The greenish lines represent the HALO flights from Cape Verde, the reddish lines those from Barbados.

.

As done for the EUREC^{4}A flights (Fig. 2b), the slope of the functional relationship between TKE and ε_w (Eq. 3) was computed for all 16 s segments of all 183 analyzed legs, Figure 9a. Here, the slope values obtained from the robust regression are listed in Figure 9a. They are very similar to the ones presented in Section 3. Also the values of the linear regressions of 0.60, 0.65, and 0.67 as determined for $\varepsilon_w \geq 10^{-5}\,m^2\,s^{-3}$, for $\varepsilon_w \geq 10^{-4}\,m^2\,s^{-3}$, and for $\varepsilon_w \geq 10^{-2}\,m^2\,s^{-3}$, respectively, resembles those from the EUREC^{4}A campaign. Moreover, the range of values for ε_w and TKE, as well as the nearly linear relationship between these two quantities, are similar to the turbulence observations made by unmanned aerial systems in the UTLS (Haghighi et al., 2024, Fig. 11). For both data sets, there is a wide spread of measured values.

As before, ℓ/C_ε can be determined and amounts to $\approx$277 (200) m (for linear regression) for the ε_w range greater than $10^{-5}\,m^2\,s^{-3}$ (green lines in Fig. 9). Assuming C_ε lying between 0.5 and 2 (depending on the Reynolds number, Wacławczyk et al. (2025)), the integral length scale ℓ amounts to about 140 (100) m which is smaller than for EUREC^{4}A. Nevertheless, a

https://doi.org/10.5194/egusphere-2026-2628
Preprint. Discussion started: 29 May 2026

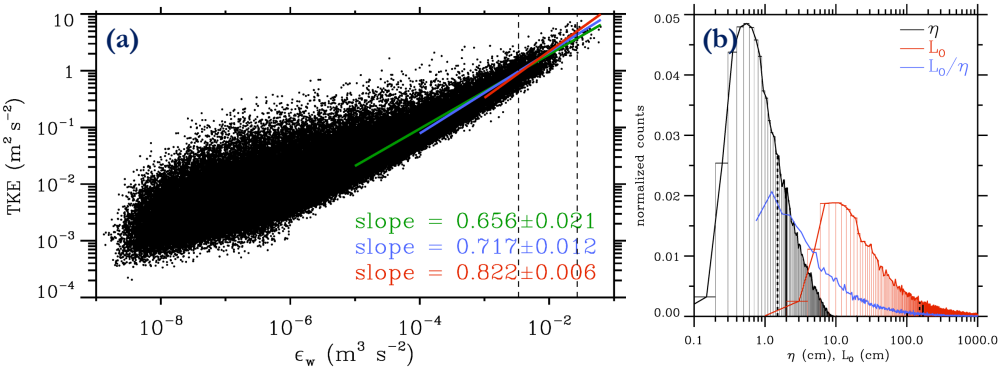

Figure 9. (a) TKE as function of ε_w for all analyzed segments of the PERCUSION research flights. The colored slope values refer to the linear regressions of $\log_{10}(\text{TKE}) = \text{f}(\log_{10}(\varepsilon_w))$ in the ε_w ranges indicated by the lengths of the respective lines, i.e., green for $\varepsilon_w \geq 10^{-5}\,\text{m}^2\,\text{s}^{-3}$, blue for $\varepsilon_w \geq 10^{-4}\,\text{m}^2\,\text{s}^{-3}$, and red for $\varepsilon_w \geq 10^{-2}\,\text{m}^2\,\text{s}^{-3}$, respectively. (b) Probability density functions of the the Kolmogorov scale η (black), the Ozmidov scale L_O (red), and the ratio L_O/η (blue line) computed from the 10 Hz BAHAMAS data. The mean and median values of the distributions are marked with thick black solid and dashed lines, respectively. The thin vertical lines in the PDFs represent the data binned according to the width of the bars, and the curves connect the values in the middle of the bars.

.

rough estimate of the buoyancy scale from Eq. 7 using $N \approx 0.01$ s and $u_{rms} \approx \sqrt{2 \times \text{TKE}}$ gives values of L_B between 140 and 400 m where TKE = 1 and 8 $\text{m}^2\,\text{s}^{-2}$ was used. So, the values of ℓ as determined from the regression curves in Fig. 9a for PERCUSION and in Fig. 4 for EUREC^{4}A are close to L_B. Both length scale, ℓ and L_B are two to three orders of magnitude larger than the Ozmidov scale L_O (Eq. 5) and and about 5 orders of magnitude larger than the Kolmogorov scale η (Eq. 4), see Fig. 9b. An airflow can be considered to be actively turbulent when the ratio L_O/η is greater than about 10, otherwise the flow is dominated by wave-like motions with little energy cascading to smaller scales, e.g. Schumann et al. (1995); Riley and Lindborg (2008). Here, 57% of all segments have ratios $\text{L}_\text{O}/\eta \geq 10$ and the median of the distribution in Fig. 9b is 104.

Figure 10 juxtaposes the PDFs of ε_w and EDR_w from the three campaigns SOUTHTRAC, EUREC^4, and PERCUSION. Although the PDFs appear to be mono-modal, their shapes and expected values differ. The expected values (medians) are 0.18 (0.12) $10^{-6}\,\text{m}^2\,\text{s}^{-3}$, 9.6 (16.6) $10^{-6}\,\text{m}^2\,\text{s}^{-3}$, and 2.24 (2.45) $10^{-6}\,\text{m}^2\,\text{s}^{-3}$ for SOUTHTRAC, EUREC^{4}A, and PERCUSION, respectively. The mean values of the respective PDFs are larger and amount to 3, 23, and $21{\cdot}10^{-5}\,\text{m}^2\,\text{s}^{-3}$, respectively. Both data sets from the tropical campaigns EUREC^{4}A and PERCUSION have larger expected values and medians and possess a larger portion of higher ε_w values compared to the SOUTHTRAC data. This finding is also reflected in the distribution of the EDR_w values. The proportion of segments with $\text{EDR}_w \geq 0.15\,\text{m}^{2/3}\,\text{s}^{-1}$ increases by one order of magnitude for EURECA and PERCUSION, respectively, compared to SOUTHTRAC. This is a plausible result as all EUREC^{4}A, and PERCUSION flights were conducted in the troposphere. Nevertheless, the absolute values of 1.3% of sections with $\text{EDR}_w \geq 0.15\,\text{m}^{2/3}\,\text{s}^{-1}$ for PERCUSION are low and indicate that most research flights were conducted under calm conditions. Nonetheless, PERCUSION flights account for a very small fraction (0.025%) of all analyzed segments in which $\text{EDR}_w \geq 0.3\,\text{m}^{2/3}\,\text{s}^{-1}$ is observed.

https://doi.org/10.5194/egusphere-2026-2628
Preprint. Discussion started: 29 May 2026

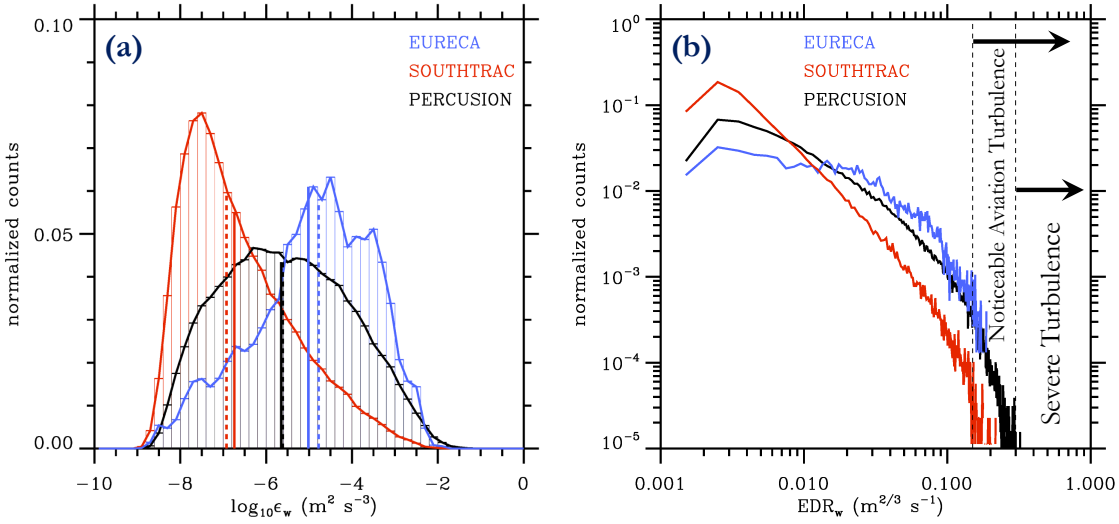

Figure 10. Probability density functions (PDFs) of ε_w (a) and EDR_w for the 183 HALO's legs during PERCUSION (black lines), for the EUREC^{4}A 100 Hz data (blue lines), and for the SOUTHTRAC 10 Hz (red lines) data as published in Dörnbrack et al. (2022). The bold vertical lines mark the expected value (solid) and the median (dashed) of the respective PDFS.

Finally, Figure 11 attempt to relate the observed EDR_w to the convective activity in the vicinity of HALO. Two metrics are used. First, one hourly TCW values are interpolated to the measurement times of the 183 constant level legs. Within the 16-second segments of the turbulence analyses, a maximum TCW value $\mathrm{TCW}_{\mathrm{MAX}}$ is identified in an area of $\pm 2°$ in latitude and longitude around the HALO positions, and its distance to HALO is estimated. All the distances are correlated with the respective EDR_w values of the previous turbulence analysis. Median values of the distance to $\mathrm{TCW}_{\mathrm{MAX}}$ are calculated in 0.02 $\mathrm{m}^{2/3}\,\mathrm{s}^{-1}$ EDR_w bins and are shown in panel (a) of Fig. 11. The second metric is the median rain rate at the HALO positions in the 16-second segments of the turbulence analyses. Here, the 30-min CMORPH data are interpolated to the measurement times of HALO. To estimate the rain rate at the HALO positions, the inverse distance weighting interpolation method (Shepard, 1968; Ahrens, 2006) with linear weighting is applied. The correlation and binning with EDR_w are performed in the exact same way as with TCW. The resulting curves for two analysis areas are shown in panel (b) of Fig. 11.

Both metrics clearly reveal that turbulence in the upper troposphere over the tropical Atlantic increases both with proximity to convective storms (panel a) and with increasing intensity (panel b). The coloring of the dots represents the median TCW values within the bins. Higher EDR_w values are associated with higher TCW values, suggesting that these values are measured closer to the ITCZ. For the PERCUSION measurements, $\mathrm{EDR}_w \geq 0.3\,\mathrm{m}^{2/3}\,\mathrm{s}^{-1}$ can occur at distances up to $\sim$200 km. Considering that these high EDR_w values occurred predominantly in the eastern Atlantic (see Fig. 8), it is evident that the strong, spatially expanded mesoscale convective systems are responsible (Stevens et al., 2026). In this sense, Fig. 11a demonstrates that the spatial range for commercial aircraft to avoid CIT can be much larger than current federal guidelines require (e.g., Hitchcock et al., 2025). This finding should be considered for potential predictions of CIT based on NWP data.

https://doi.org/10.5194/egusphere-2026-2628
Preprint. Discussion started: 29 May 2026

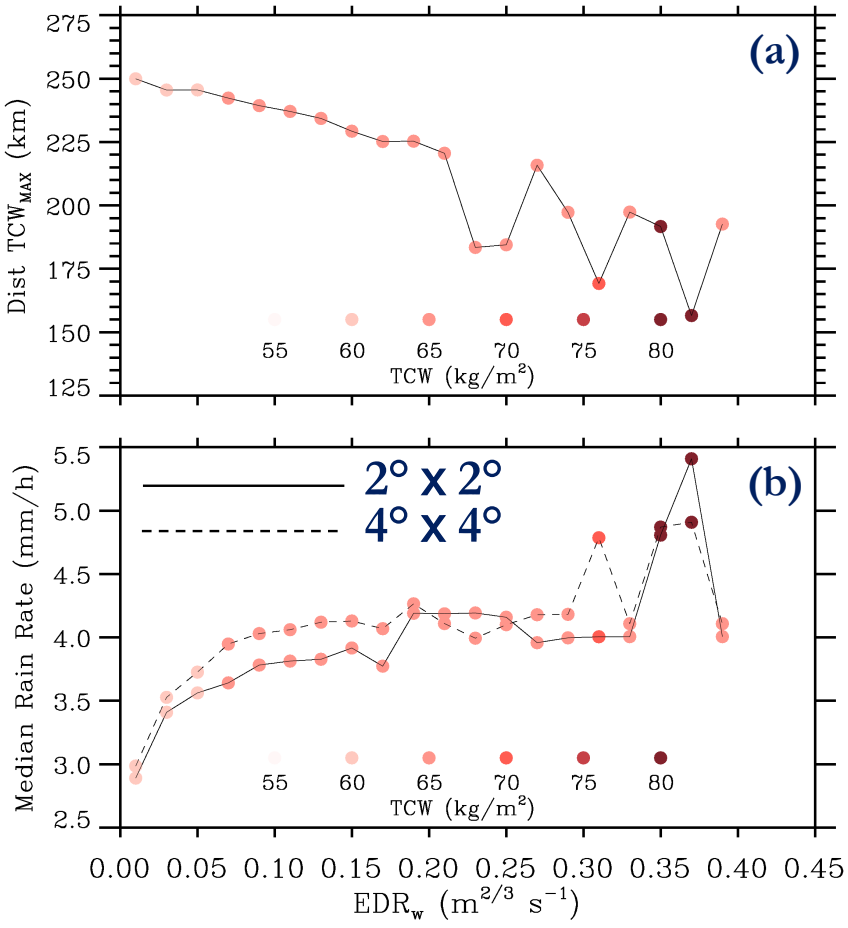

Figure 11. (a) Distance to the maximum of total column water (TCW_{MAX}) located in an area $\pm 2^{\circ}$ in latitude and longitude from HALO's positions as function of EDR_w. The distances to TCW_{MAX} are median values calculated within EDR_w intervals divided into bins with a length of 0.02 $m^{2/3}$ s^{-1}. (b) Median rain rates at the HALO positions in the same binned EDR_w intervals as in (a). Median rain rates at the HALO locations are determined by the "inverse distance weighting" interpolation method, employing temporally interpolated 30-minute CMORPH rainfall intensity data (Xie et al., 2017) in the specified areas, each of which is centered at the HALO locations. The colored dots represent the respective median TCW values of the 20 EDR_w bins.

5 Doldrums and Upper-level Turbulence

This section examines whether the observed turbulence intensity in the upper troposphere is correlated with flow characteristics of the lower atmospheric layers. For this purpose, the 89 circles flown during PERCUSION are investigated. Figure 12 is a visual representation of the location of the circular flight legs in relation to the location of the northern edge of the ITCZ.

https://doi.org/10.5194/egusphere-2026-2628
Preprint. Discussion started: 29 May 2026

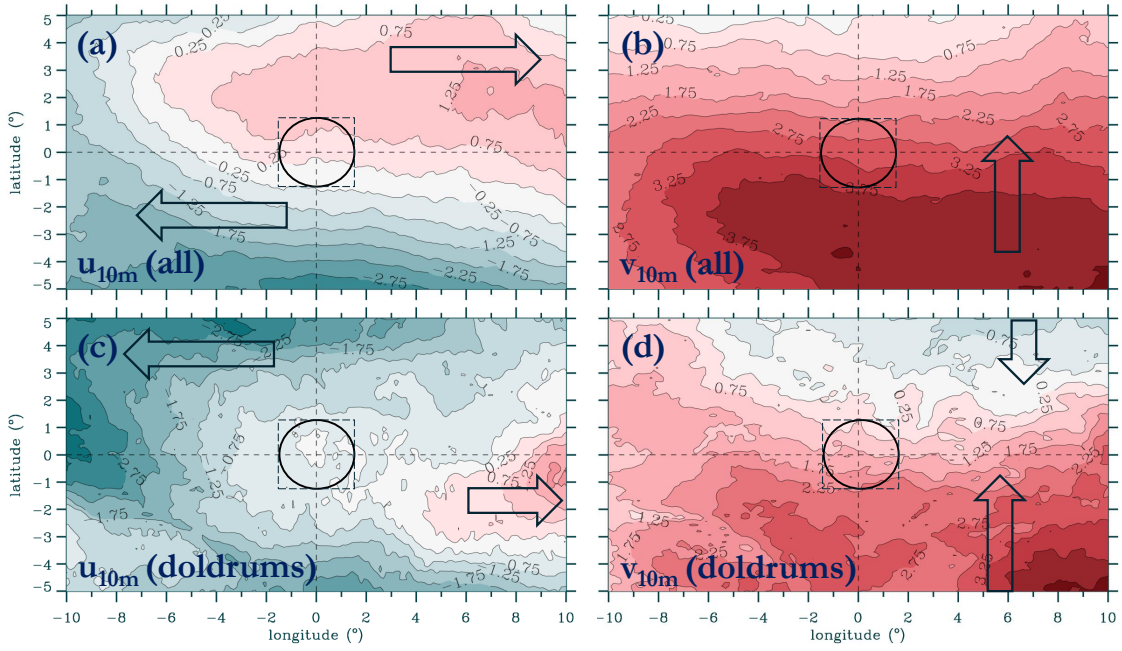

Figure 12. Circle-centered composites of $u_{10\,\mathrm{m}}$ (a, c) and $v_{10\,\mathrm{m}}$ (b, d) for the 89 circles flown during PERCUSION (upper row). Lower row: circle-centered composites for the 15 circular flight legs where $|u_{10\,\mathrm{m}}| \leq 3\,\mathrm{m\,s^{-1}}$. Here $|u_{10\,\mathrm{m}}|$ is the mean along the circular flight legs. The black circles in the center represent the large circular flight legs with a diameter of 200 km, and the squares enclose the area where the IFS data were collected to determine whether or not a flight leg was located above the doldrums. Data: Hourly IFS data interpolated in time onto the HALO flight tracks.

.

Panels (a) and (b) show the circle-centered composites of $u_{10\,\mathrm{m}}$ and $v_{10\,\mathrm{m}}$ averaged over all 89 circles, while panels (c) and (d) show the composites for the 15 circular flight segments[3] where the doldrums criterion of $|u_{10\,\mathrm{m}}| \leq 3\,\mathrm{m\,s^{-1}}$ was applied to the interpolated $|u_{10\,\mathrm{m}}|$ values averaged along the flight legs. The difference is striking: while the composite means of all 89 circles is clearly within the ITCZ with prevailing southerly winds, the 15 circles of the doldrums are closer to the convergence zone at the northern edge of the ITCZ, where the mean value $v_{10\,\mathrm{m}}$ is smaller and $u_{10\,\mathrm{m}} \approx 0$ lies within the circles. The composites presented in Fig. 12c and d agree qualitatively very well with the composite view of the ITCZ retrieved from the global storm-resolving numerical simulations by Klocke et al. (2017): There, the location of the calm regions of the doldrums coincides with a nearly vanishing meridional wind component $v_{10\,\mathrm{m}}$ (Klocke et al., 2017, their panels b and c of Fig. 2 for August). Since only four circles were identified as belonging to the doldrums during flights over the eastern Atlantic (two of them are the small circles that were always flown close to Cape Verde), the proximity of flights to the trade wind zone over the

[3]The identified circular flight legs of the doldrums are 0818-1, 0822-5, 0825-3, 0827-2, 0906-1, 0907-2, 0912-2+3, 0914-5, 0921-4+5, 0924-2+3, 0928-2+3, where the number following MMDD denotes the number according to the orderin which the circular legs were flown during the research flight. The circles on August 22 and 27 are small diameter circles.

https://doi.org/10.5194/egusphere-2026-2628
Preprint. Discussion started: 29 May 2026

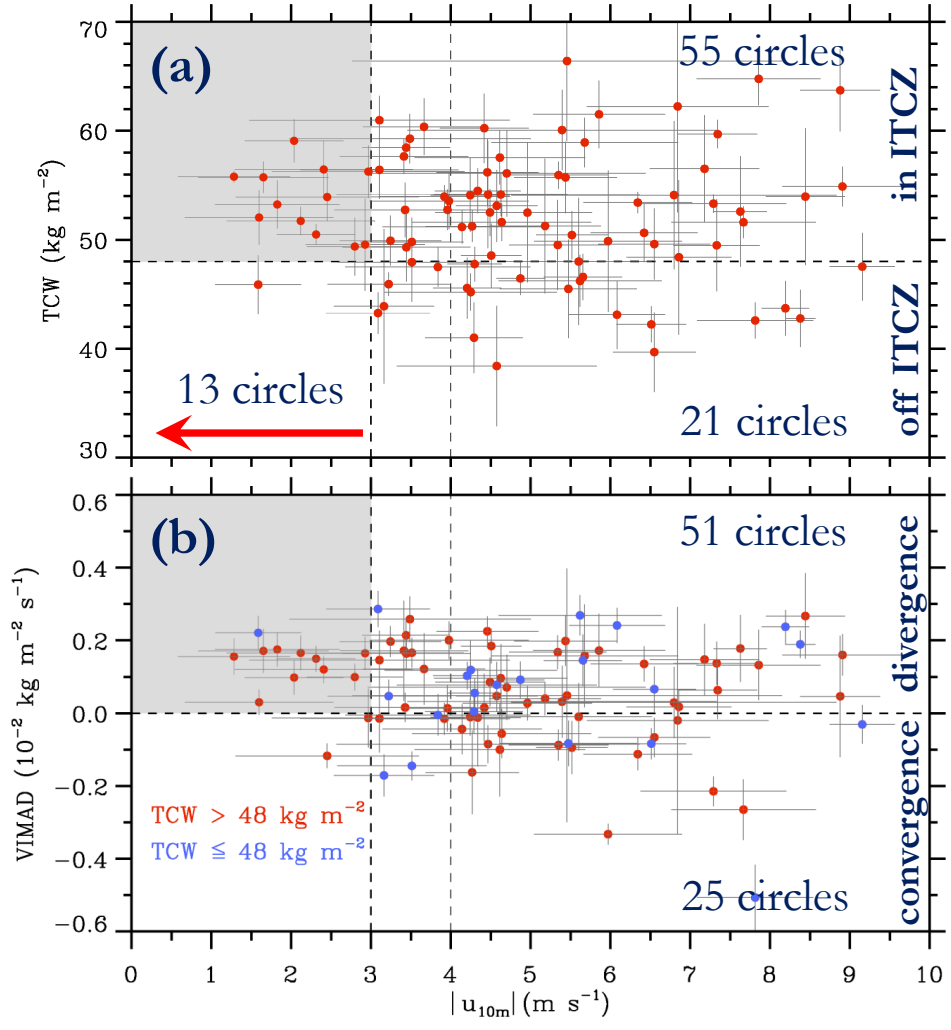

Figure 13. TCW, VIMAD as function of $u_{10\,\mathrm{m}}$ for the 89 circles flown during PERCUSION. Dots: values of TCW, VIMAD, and $|u_{10\,\mathrm{m}}|$ as are area averages over squares enclosing the circles. The vertical and horizontal lines indicate the respective standard deviations. Data: Hourly IFS data interpolated in time onto the HALO flight tracks.

.

western Atlantic could explain the different flow patterns that dominate the composite analysis for the doldrums in Fig. 12c and d.

Figure 13 presents the dependence of TCW (panel a) and VIMAD (b) as function of $|u_{10\,\mathrm{m}}|$. The 2D fields of hourly values from the IFS were interpolated to the respective times of the HALO observations. The actual values of TCW, VIMAD, and $|u_{10\,\mathrm{m}}|$ (dots in Fig. 13) are area averages over squares enclosing the circles; the vertical and horizontal lines indicate the respective standard deviations. There are 13 (30) circles in which the area-averaged values $|u_{10\,\mathrm{m}}|$ was less than 3 (4) m s^{-1}.

https://doi.org/10.5194/egusphere-2026-2628
Preprint. Discussion started: 29 May 2026

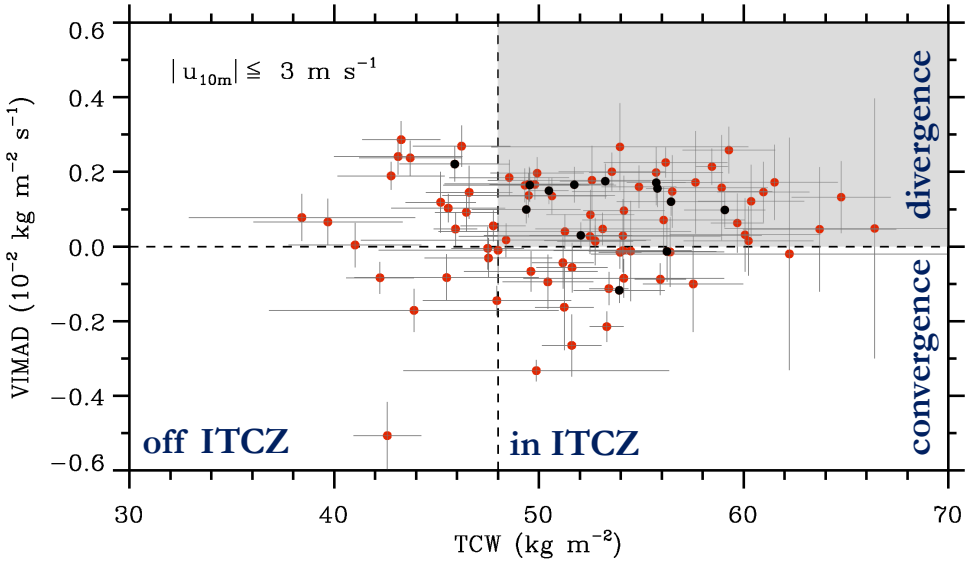

Figure 14. VIMAD as function of TCW as area averages of the 89 circles flown by HALO. The black colored dots denote circles with low-level wind $|u_{10\,\mathrm{m}}| \leq 3\,\mathrm{m\,s^{-1}}$, all others have greater $|u_{10\,\mathrm{m}}|$ (red). The quadrants mark if the quantities are inside/outside the ITCZ (TCW $\gtrless 48\,\mathrm{kg\,m^{-2}}$) and if they contain a convergent/divergent mass flow (VIMAD $\lessgtr 0$). The vertical and horizontal lines indicate the respective standard deviations. Data: Hourly IFS data interpolated in time onto the HALO flight tracks.

.

Most of these circles are located within the ITCZ (taking into account a threshold value of TCW $= 48\,\mathrm{kg\,m^{-2}}$), implying that they are potential doldrums, Fig. 13a. The total number of circles within the ITCZ is 67 and only 22 circular legs were placed outside the ITCZ. Altogether, 55 circular flights within the ITCZ had values $|u_{10\,\mathrm{m}}| > 3\,\mathrm{m\,s^{-1}}$. Nevertheless, even values outside the ITCZ have large standard deviations of TCW, meaning that the HALO flight legs may have been at the edge or even partially within the ITCZ. Most of the potential doldrums occur when VIMAD is positive, i.e. under divergent flow conditions, Fig. 13b. And again, the majority of these quantities are located inside the ITCZ as indicated by the red circles in panel (b).

The direct dependence of TCW and VIMAD is visualized in Figure 14, where the upper right quadrant combines all values that would confirm the hypothesis about doldrums: *divergent* air flow *inside* the ITCZ. It is obvious that only 10 out of 47 points in the upper right quadrant satisfy the strict doldrum condition of $|u_{10\,\mathrm{m}}| \leq 3\,\mathrm{m\,s^{-1}}$. Using the weaker condition of $|u_{10\,\mathrm{m}}| \leq 4\,\mathrm{m\,s^{-1}}$ the number would increas to 21.

Furthermore, weak low-level winds also occurred outside the ITCZ and under convergent conditions. It must be noted, that the variability in TCW, VIMAD, and $|u_{10\,\mathrm{m}}|$ inside the investigated areas is surprisingly large, considering that hourly IFS data interpolated into a 0.25° latitude/longitude grid are used and the examined circle had diameters of 200 km only. This large variability reflect, on the one hand, the rapid spatial variations in the tropical troposphere and, on the other hand, the difficulty of reproducing these atmospheric conditions with the results of an operational NWP model. So, these presented results should

https://doi.org/10.5194/egusphere-2026-2628
Preprint. Discussion started: 29 May 2026

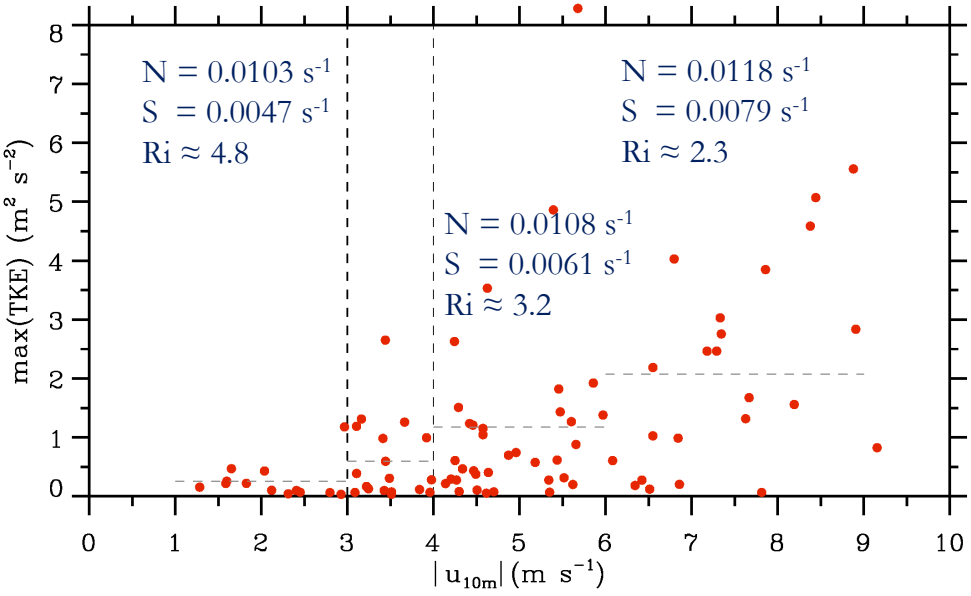

Figure 15. Maximum TKE observed by BAHAMAS along the 89 circles as function of the low-level wind $u_{10\,\mathrm{m}}$ as determined from IFS data in area enclosing the circular legs. Vertical dashed line marks the strict condition ($|u_{10\,\mathrm{m}}| \leq 3\,\mathrm{m\,s^{-1}}$) for the doldrums. The stepwise ascending horizontal lines represent the $\mathrm{TKE_{MAX}}$ values, which were calculated by averaging all values in the interval corresponding to the length in $|u_{10\,\mathrm{m}}|$.

be judged with care and either high-resolution numerical simulations or the evaluation of other PERCUSION data sets should be considered to provide statistically more stable results.

Finally, and based solely on the previous results from the IFS analyses, Figure 15 shows the dependence of the maximum measured TKE values $\mathrm{TKE_{MAX}}$ along the 89 HALO circles as a function of $|u_{10\,\mathrm{m}}|$. The encouraging result is that, over all, $\mathrm{TKE_{MAX}}$ increases with greater $|u_{10\,\mathrm{m}}|$, see the dashed horizontal lines that represent the average $\mathrm{TKE_{MAX}}$ over the respective $|u_{10\,\mathrm{m}}|$ intervals.

The really small $\mathrm{TKE_{MAX}}$ values less than $0.5\,\mathrm{m^2\,s^{-2}}$ for $|u_{10\,\mathrm{m}}| \leq 3\,\mathrm{m\,s^{-1}}$ represent the doldrum circles and are mainly associated with areas inside the ITCZ and divergent motions as shown before. A similar dependence as shown in Fig. 15 was also found for the maximum of EDR_w as function of $|u_{10\,\mathrm{m}}|$ (not shown). Despite this clear result, low $\mathrm{TKE_{MAX}}$ in the upper troposphere for weak low-level winds, it must be admitted that the reversal of this relationship does not apply in the tropics. There are certainly small $\mathrm{TKE_{MAX}}$ values when high $|u_{10\,\mathrm{m}}|$ values are present in the same area. In this sense, the result presented in Fig. 15 can only be considered a preliminary, tentative indication that there is a direct connection between the doldrums and reduced turbulence in the upper troposphere of the ITCZ.

In the Introduction, the hypothesis was formulated that descending air flows above the doldrums are associated with thermal stabilization and a reduction in turbulence in the upper troposphere. However, the numbers shown in Fig. 15 indicate that the

https://doi.org/10.5194/egusphere-2026-2628
Preprint. Discussion started: 29 May 2026

mean buoyancy frequency N of the three $u_{10\,\mathrm{m}}$ intervals is lowest over the doldrums and that N increases by approximately 10% with higher values of $|u_{10\,\mathrm{m}}|$. Interestingly, the shear values S also increase with $|u_{10\,\mathrm{m}}|$, specifically by about 50%. This difference in the ambient atmospheric conditions leads to higher Richardson numbers above the doldrums, a possible indication of observed reduced upper tropospheric turbulence.

6 Summary and Conclusion

Airborne measurements collected by the German research aircraft HALO during the PERCUSION campaign in summer 2024 are analyzed to assess the upper-level turbulence over the Atlantic ITCZ. Combining 10 Hz-resolution BAHAMAS in-situ winds with ECMWF IFS diagnostics, the study evaluates energy dissipation rates ε_w (or $\mathrm{EDR}_w \equiv \varepsilon_w^{1/3}$), turbulent kinetic energy (TKE), and spectral behavior across multiple flight campaigns to compare upper-tropospheric turbulence over the tropical Atlantic to mid-latitude observations. Moreover, this study pursues a hypothesis based on recently observed subsidence and low-level divergence in doldrums (Windmiller, 2024): Are doldrums associated with a thermally stabilized, less turbulent upper troposphere? The PERCUSION measurements find a tentative link: Weak near-surface winds within the ITCZ do indeed coincide with reduced TKE in the upper troposphere. Moreover, the analysis of the ambient atmospheric conditions at flight level reveals smaller shear and larger Richardson numbers for the identified areas of the doldrums. Since most of the doldrums were found at the northern edge of the ITCZ over the western Atlantic, convective activity may not have been as intense or as deep-reaching as over the eastern Atlantic. There, deep convective storms might have led to a stronger vertical shear in the outflow regions in the upper troposphere. This East-West asymmetry of convective activity was also mentioned the recent overview paper by Stevens et al. (2026).

To consolidate the investigation of the 10 Hz PERCUSION data, high-resolution (100 Hz) and default (10 Hz) BAHAMAS wind measurements from selected flight legs over the tropical Atlantic during EUREC^{4}A are analyzed. The power spectra of vertical wind S_w from the 100 Hz data align well with the expected Kolmogorov $-5/3$ slope in the inertial subrange, while the 10 Hz data show similar S_w magnitudes but slightly flatter slopes at high frequencies. Both EDR_w and TKE are computed for the same flight segments. The spatial distributions and statistical properties of both quantities from 10 and 100 Hz data are in strong agreement, confirming the validity of the lower-resolution data for turbulence studies. The probability density functions of ε_w show that EUREC^{4}A (tropical troposphere) has a higher frequency and magnitude of MoG turbulence compared to SOUTHTRAC (lower stratosphere), as expected from the different atmospheric regimes. Severe turbulence events are rare in both campaigns. A robust relationship between TKE and ε_w is observed, with regression slopes of the the log-log plots close to the theoretical 2/3 value derived from turbulence theory. The close agreement between 10 and 100 Hz BAHAMAS data demonstrates that the 10 Hz data set is sufficient and reliable for characterizing atmospheric turbulence in subsequent analyses, such as those performed for the PERCUSION campaign.

Twenty-three HALO research flights were conducted between the equator and 20°N, from 60°W to 20°W in August/September 2024. These PERCUSION flights, although planned and conducted for totally different reasons (Groß et al., 2026), were investigated to analyze the turbulence in the upper troposphere over the tropical eastern and western Atlantic. In these re-

https://doi.org/10.5194/egusphere-2026-2628
Preprint. Discussion started: 29 May 2026

search flights 183 constant-altitude legs were identified, mostly flown between 13 and 15 km altitude, all within the tropical troposphere. Atmospheric background conditions (stratification, shear, Richardson number) were characterized using ECMWF IFS reanalysis interpolated along the flight tracks. The PERCUSION flights occurred in a thermally stable troposphere (buoyancy frequency $N \approx 0.01\,\mathrm{s}^{-1}$), with lower stratification than SOUTHTRAC (stratosphere, $N \approx 0.02\,\mathrm{s}^{-1}$). Shear values were moderate; most flight legs showed low vertical shear and high Richardson numbers, indicating stable, less turbulence-prone conditions.

Power spectra of vertical wind S_w showed variability between flights, with higher turbulence over the eastern Atlantic (flights from Cape Verde) and lower turbulence over the western Atlantic (flights from Barbados). The S_w spectra partly followed the Kolmogorov $-5/3$ law in the inertial subrange, but flattened at higher frequencies. Higher turbulence ($\mathrm{EDR}_w > 0.3\,\mathrm{m}^{2/3}\,\mathrm{s}^{-1}$) and TKE values were found more frequently in the eastern Atlantic and closer to the equator. TKE values reached up to $8\,\mathrm{m}^2\,\mathrm{s}^{-2}$ in the east, while the HALO flights over the western Atlantic resembled earlier EUREC^{4}A observations. The relationship between TKE and ε_w in the log-log plot was nearly linear (slope $\sim 2/3$), consistent with turbulence theory and the previous findings of EUREC^{4}A. Compared to SOUTHTRAC (lower stratosphere), both PERCUSION and EUREC4A (upper troposphere in the tropics) had higher mean and median ε_w and EDR_w values, with a larger fraction of segments showing higher turbulence. However, strong turbulence ($\mathrm{EDR}_w \geq 0.3\,\mathrm{m}^{2/3}\,\mathrm{s}^{-1}$) remained rare ($< 1\%$ of segments) but could occur up to 200 km from the nearest convective core, especially in the eastern Atlantic, suggesting a spatially extensive influence of mesoscale convective systems.

Moreover, this study investigates whether there is a direct connection between the doldrums - regions of calm, low-level winds within the Atlantic ITCZ - and reduced turbulence in the upper troposphere above these areas. The analysis focuses on 89 circular flight legs flown during the PERCUSION campaign. Using the conditions $|u_{10\mathrm{m}}| \leq 3\,\mathrm{m\,s}^{-1}$ underneath the circles, the location of the doldrums is close to the northern edge of the ITCZ. Out of 89 circles, 15 met the strict doldrum criterion, mostly located within the ITCZ (total column water $\mathrm{TCW} > 48\,\mathrm{kg\,m}^{-2}$) and under divergent flow conditions vertically integrated mass divergence, $\mathrm{VIMAD} > 0$. The maximum turbulent kinetic energy ($\mathrm{TKE}_{\mathrm{MAX}}$) along each circle was compared to the corresponding low-level wind speed. Doldrum circles generally showed lower upper-tropospheric turbulence ($\mathrm{TKE}_{\mathrm{MAX}} < 0.5\,\mathrm{m}^2\,\mathrm{s}^{-2}$). Some circles with weak low-level winds also occurred outside the ITCZ or under convergent conditions, highlighting variability in atmospheric conditions. Moreover, the relationship between $\mathrm{TKE}_{\mathrm{MAX}}$ and $|u_{10\mathrm{m}}|$ was not exclusive: Weak upper-level turbulence has also been observed for large near-surface winds, which is often associated with mesoscale convection. During PERCUSION, regional differences between the eastern and western tropical Atlantic have been observed.

Significant spatial variability in TCW, VIMAD, and $|u_{10\mathrm{m}}|$ was found even within small areas, reflecting both rapid changes in the tropical troposphere and the limitations of model resolution. Furthermore, the analysis of the column-integrated divergence from the more than 1100 dropsondes released along the circular flight legs reveals a considerable vertical variability, see Fig. 11 of Gloeckner et al. (2025). Given that the values shown are not weighted by atmospheric density, it is difficult to assess whether the VIMAD results of this study are consistent with the observations of Gloeckner et al. (2025). The study's findings

https://doi.org/10.5194/egusphere-2026-2628
Preprint. Discussion started: 29 May 2026

suggest that further research using higher-resolution simulations or additional datasets is needed to confirm, deny, or at least to clarify the relationship between the doldrums and turbulence in the upper troposphere.

Data availability. The ERA5 reanalysis data is available on the Copernicus Climate Change Service (C3S) Climate Data Store: https://doi.org/10.24381/cds.143582cf (Hersbach et al., 2020). The CMORPH precipitation rate data product is freely available (Xie et al., 2019). The BAHAMAS in situ observations from the research aircraft HALO are stored in the HALO data base https://halo-db.pa.op.dlr.de/ under the mission entry PERCUSION.

Author contributions. AD formulated and designed the study and performed the analysis. AD, AG, CM, and CCS wrote the manuscript.

Competing interests. The contact author has declared that neither of the authors has any competing interests.

Acknowledgements. This study was inspired by a presentation of Julia Windmiller at the 24th Conference on Atmospheric and Oceanic Fluid Dynamics & 22nd Conference on Middle Atmosphere, 24-28 June 2024, Burlington, VT, USA. I would like to express my sincere thanks to her for the opportunity, arising from her lecture, to explore parts of the meteorology in the tropics. Financially, the HALO flights during PERCUSION were supported by the entire ORCESTRA consortium (Stevens et al., 2026). The unique analysis of the 100-Hz BAHAMAS data from EUREC^{4}A was funded by the MPI Hamburg. AD thanks Andreas Schäfler and Konstantin Krüger from the DLR Institute of Atmospheric Physics for their careful reviews of an early version of this manuscript.

https://doi.org/10.5194/egusphere-2026-2628
Preprint. Discussion started: 29 May 2026

References

Ahrens, B.: Distance in spatial interpolation of daily rain gauge data, Hydrology and Earth System Sciences, 10, 197–208, https://doi.org/10.5194/hess-10-197-2006, 2006.

Atlas, R. and Bretherton, C. S.: Aircraft observations of gravity wave activity and turbulence in the tropical tropopause layer: prevalence, influence on cirrus clouds, and comparison with global storm-resolving models, Atmospheric Chemistry and Physics, 23, 4009–4030, https://doi.org/10.5194/acp-23-4009-2023, 2023.

Atlas, R., Podglajen, A., Wilson, R., Hertzog, A., and Plougonven, R.: Turbulence in the tropical stratosphere, equatorial Kelvin waves, and the quasi-biennial oscillation, Proceedings of the National Academy of Sciences, 122, e2409791 122, https://doi.org/10.1073/pnas.2409791122, 2025.

Atlas, R., Ueyama, R., Kim, S.-H., Bui, P., Dean-Day, J., Li, Y., Dykema, J., Keutsch, F., Weinzierl, B., Dollner, M., and Podglajen, A.: Upper-Level Turbulence in the North American and Asian Summer Monsoon Regions Sampled in Recent Aircraft Campaigns, Geophysical Research Letters, 53, e2025GL118 648, https://doi.org/https://doi.org/10.1029/2025GL118648, e2025GL118648 2025GL118648, 2026.

Bechtold, P., Bramberger, M., Dörnbrack, A., Leutbecher, M., and Isaksen, L.: Experimenting with a Clear Air Turbulence (CAT) Index from the IFS, ECMWF Technical Memoranda, 874, https://doi.org/10.21957/4l34tqljm, 2021a.

Bechtold, P., Bramberger, M., Dörnbrack, A., Isaksen, L., and Leutbecher, M.: Forecasting Clear-Air Turbulence, ECMWF Newsletter, 169, 32–37, 2021b.

Bramberger, M., Dörnbrack, A., Wilms, H., Ewald, F., and Sharman, R.: Mountain-Wave Turbulence Encounter of the Research Aircraft HALO above Iceland, Journal of Applied Meteorology and Climatology, 59, 567 – 588, https://doi.org/10.1175/JAMC-D-19-0079.1, 2020.

Dörnbrack, A., Bechtold, P., and Schumann, U.: High-Resolution Aircraft Observations of Turbulence and Waves in the Free Atmosphere and Comparison With Global Model Predictions, Journal of Geophysical Research: Atmospheres, 127, e2022JD036 654, https://doi.org/https://doi.org/10.1029/2022JD036654, e2022JD036654 2022JD036654, 2022.

Giez, A., Mallaun, C., Zöger, M., Dörnbrack, A., and Schumann, U.: Static Pressure from Aircraft Trailing-Cone Measurements and Numerical Weather-Prediction Analysis, Journal of Aircraft, 54, 1728–1737, https://doi.org/10.2514/1.C034084, 2017.

Giez, A., Zöger, M., Dreiling, V., and Mallaun, C.: Static source error calibration of a nose boom mounted air data system on an atmospheric research aircraft using the trailing cone method, Tech. Rep. 2019-07, DLR, Oberpfaffenhofen, https://elib.dlr.de/135789/, 2019.

Giez, A., Mallaun, C., Nenakhov, V., and Zöger, M.: Calibration of a Nose Boom Mounted Airflow Sensor on an Atmospheric Research Aircraft by Inflight Maneuvers, Tech. Rep. 2021-17, DLR, Oberpfaffenhofen, https://elib.dlr.de/145704/, 2021.

Giez, A., Zöger, M., Mallaun, C., Nenakhov, V., Schimpf, M., Grad, C., Numberger, A., and Raynor, K.: Determination of the Measurement Errors for the HALO Basic Data System BAHAMAS by Means of Error Propagation, Tech. Rep. 2022-27, DLR, Oberpfaffenhofen, https://doi.org/https://doi.org/10.57676/5rdc-q708, 2022.

Giez, A., Mallaun, C., Nenakhov, V., and Zöger, M.: Calibration of a Nose Boom Mounted Airflow Sensor on an Atmospheric Research Aircraft by Inflight Maneuvers incl. Appendix A, Tech. Rep. 2025-17, DLR, Oberpfaffenhofen, https://doi.org/https://doi.org/10.57676/7wf2-dk78, 2025.

Gisinger, S., Bramberger, M., Dörnbrack, A., and Bechtold, P.: Severe Convectively Induced Turbulence Hitting a Passenger Aircraft and Its Forecast by the ECMWF IFS Model, Geophysical Research Letters, 51, e2024GL113 037, https://doi.org/https://doi.org/10.1029/2024GL113037, e2024GL113037 2024GL113037, 2024.

https://doi.org/10.5194/egusphere-2026-2628
Preprint. Discussion started: 29 May 2026

Gloeckner, H. M., Mieslinger, T., Robbins-Blanch, N., George, G., Kluft, L., Kölling, T., Bony, S., Windmiller, J., and Stevens, B.: BEACH: Barbados and Eastern Atlantic Combined High-altitude dropsonde datasets, Earth System Science Data Discussions, 2025, 1–35, https://doi.org/10.5194/essd-2025-647, 2025.

Groß, S., Ewald, F., Stevens, B., Wirth, M., Dekoutsidis, G., Ehrlich, A., Kouklaki, D., Krüger, K., Rosenburg, S., Volkmer, L., von Bismark, J., Hirsch, L., Luebke, A. E., Marinou, E., Mayer, B., Pinol Sole, M., Wendisch, M., Windmiller, J., Amiridis, V., Koopman, R., Kubota, T., and Rapp, M.: Persistent EarthCARE underflight studies of the ITCZ and organized convection (PERCUSION): Contribution to EarthCARE Validation, EGUsphere, 2026, 1–41, https://doi.org/10.5194/egusphere-2026-112, 2026.

Haghighi, A. N., Nolin, R. D., Pundsack, G. D., Craine, N., Stratsilatau, A., and Bailey, S. C. C.: High-altitude balloon-launched uncrewed aircraft system measurements of atmospheric turbulence and qualitative comparison with infrasound microphone response, Atmospheric Measurement Techniques, 17, 4863–4889, https://doi.org/10.5194/amt-17-4863-2024, 2024.

Hersbach, H., Bell, B., Berrisford, P., Hirahara, S., Horányi, A., Muñoz-Sabater, J., Nicolas, J., Peubey, C., Radu, R., Schepers, D., Simmons, A., Soci, C., Abdalla, S., Abellan, X., Balsamo, G., Bechtold, P., Biavati, G., Bidlot, J., Bonavita, M., Chiara, G. D., Dahlgren, P., Dee, D., Diamantakis, M., Dragani, R., Flemming, J., Forbes, R., Fuentes, M., Geer, A., Haimberger, L., Healy, S., Hogan, R. J., Hólm, E., Janisková, M., Keeley, S., Laloyaux, P., Lopez, P., Lupu, C., Radnoti, G., de Rosnay, P., Rozum, I., Vamborg, F., Villaume, S., and Thépaut, J. N.: The ERA5 global reanalysis, Quarterly Journal of the Royal Meteorological Society, 146, 1999–2049, https://doi.org/10.1002/qj.3803, 2020.

Hitchcock, S. M., Lane, T. P., Deierling, W., Sharman, R. D., Trier, S. B., and Homeyer, C. R.: Spatial Patterns of Turbulence near Thunderstorms, Bulletin of the American Meteorological Society, 106, E1 – E22, https://doi.org/10.1175/BAMS-D-23-0142.1, 2025.

Jaffeux, L., Lothon, M., Couvreux, F., Bouniol, D., Cayez, G., Joly, L., Burgalat, J., De Saint Leger, C., Bellec, H., Henry, O., Chbib, D., Jiang, T., and Bony, S.: The MAESTRO turbulence dataset derived from the SAFIRE ATR42 aircraft, Earth System Science Data Discussions, 2025, 1–31, https://doi.org/10.5194/essd-2025-586, 2025.

Khani, S. and Waite, M. L.: Buoyancy scale effects in large-eddy simulations of stratified turbulence, Journal of Fluid Mechanics, 754, 75–97, https://doi.org/10.1017/jfm.2014.381, 2014.

Kim, J. and Son, S.-W.: Tropical Cold-Point Tropopause: Climatology, Seasonal Cycle, and Intraseasonal Variability Derived from COSMIC GPS Radio Occultation Measurements, Journal of Climate, 25, 5343 – 5360, https://doi.org/10.1175/JCLI-D-11-00554.1, 2012.

Kim, S.-H., Ueyama, R., Atlas, R., Dean-Day, J., Bui, P., Smith, J. B., Podglajen, A., and Homeyer, C. R.: Atmospheric Turbulence in the Upper Troposphere and Lower Stratosphere From Airborne Observations During the DCOTSS Field Campaign, Journal of Geophysical Research: Atmospheres, 130, e2025JD044 556, https://doi.org/https://doi.org/10.1029/2025JD044556, e2025JD044556 2025JD044556, 2025.

Klocke, D., Brueck, M., Hohenegger, C., and Stevens, B.: Rediscovery of the doldrums in storm-resolving simulations over the tropical Atlantic, Nature Geosciences, 10, 891–896, https://doi.org/https://doi.org/10.1038/s41561-017-0005-4, 2017.

Ko, H.-C., Chun, H.-Y., and Bechtold, P.: Evaluation and Improvement of the ECMWF Aviation Turbulence Forecasts, Journal of Geophysical Research: Atmospheres, 130, e2024JD043 158, https://doi.org/https://doi.org/10.1029/2024JD043158, e2024JD043158 2024JD043158, 2025.

Kolmogorov, A.: Local Structure of Turbulence in an Incompressible Viscous Fluid at Very Large Reynolds Numbers, Dokl. Akad. Nauk SSSR, 30, 299–301, 1941.

https://doi.org/10.5194/egusphere-2026-2628
Preprint. Discussion started: 29 May 2026

Krautstrunk, M. and Giez, A.: The transition from FALCON to HALO era airborne atmopheric research, in: Atmospheric Physics - Background - Methods - Trends, edited by Schumann, U., p. 609-624, Springer, Heidelberg, https://doi.org/10.1007/978-3-642-30183-4_37, 2012.

Köhler, L., Green, B., and Stephan, C. C.: Comparing Loon Superpressure Balloon Observations of Gravity Waves in the Tropics With Global Storm-Resolving Models, Journal of Geophysical Research: Atmospheres, 128, e2023JD038 549, https://doi.org/https://doi.org/10.1029/2023JD038549, e2023JD038549 2023JD038549, 2023.

Lane, T. P. and Sharman, R. D.: Some Influences of Background Flow Conditions on the Generation of Turbulence due to Gravity Wave Breaking above Deep Convection, Journal of Applied Meteorology and Climatology, 47, 2777 – 2796, https://doi.org/10.1175/2008JAMC1787.1, 2008.

Nugent, J. M., Bretherton, C. S., and Blossey, P. N.: What Sets the Tropical Cold Point in GSRMs During Boreal Winter? Overshooting Convection Versus Cirrus Lofting, Earth and Space Science, 12, e2024EA003 887, https://doi.org/https://doi.org/10.1029/2024EA003887, e2024EA003887 2024EA003887, 2025.

Oncley, S. P., Friehe, C. A., Larue, J. C., Businger, J. A., Itsweire, E. C., and Chang, S. S.: Surface-Layer Fluxes, Profiles, and Turbulence Measurements over Uniform Terrain under Near-Neutral Conditions, Journal of the Atmospheric Sciences, 53, 1029 – 1044, https://doi.org/10.1175/1520-0469(1996)053<1029:SLFPAT>2.0.CO;2, 1996.

Ozmidov, R. V.: On the turbulent exchange in a stably stratified ocean, Izv. Akad. Nauk SSSR, 1, 861–871, 1965.

Piper, M. and Lundquist, J. K.: Surface Layer Turbulence Measurements during a Frontal Passage, Journal of the Atmospheric Sciences, 61, 1768 – 1780, https://doi.org/10.1175/1520-0469(2004)061<1768:SLTMDA>2.0.CO;2, 2004.

Rapp, M., Kaifler, B., Dörnbrack, A., Gisinger, S., Mixa, T., Reichert, R., Kaifler, N., Knobloch, S., Eckert, R., Wildmann, N., Giez, A., Krasauskas, L., Preusse, P., Geldenhuys, M., Riese, M., Woiwode, W., Friedl-Vallon, F., Sinnhuber, B.-M., de la Torre, A., Alexander, P., Hormaechea, J. L., Janches, D., Garhammer, M., Chau, J. L., Conte, J. F., Hoor, P., and Engel, A.: SOUTHTRAC-GW: An Airborne Field Campaign to Explore Gravity Wave Dynamics at the World's Strongest Hotspot, Bulletin of the American Meteorological Society, 102, E871 – E893, https://doi.org/10.1175/BAMS-D-20-0034.1, 2021.

Riley, J. J. and Lindborg, E.: Stratified Turbulence: A Possible Interpretation of Some Geophysical Turbulence Measurements, Journal of the Atmospheric Sciences, 65, https://doi.org/10.1175/2007JAS2455.1, 2008.

Rodriguez Imazio, P., Dörnbrack, A., Urzua, R. D., Rivaben, N., and Godoy, A.: Clear Air Turbulence Observed Across a Tropopause Fold Over the Drake Passage — A Case Study, Journal of Geophysical Research: Atmospheres, 127, e2021JD035 908, https://doi.org/https://doi.org/10.1029/2021JD035908, e2021JD035908 2021JD035908, 2022.

Rodriguez Imazio, P., Mininni, P. D., Godoy, A., Rivaben, N., and Dörnbrack, A.: Not All Clear Air Turbulence Is Kolmogorov—The Fine-Scale Nature of Atmospheric Turbulence, Journal of Geophysical Research: Atmospheres, 128, e2022JD037 491, https://doi.org/https://doi.org/10.1029/2022JD037491, e2022JD037491 2022JD037491, 2023.

Schumann, U.: The Horizontal Spectrum of Vertical Velocities near the Tropopause from Global to Gravity Wave Scales, Journal of the Atmospheric Sciences, 76, 3847 – 3862, https://doi.org/10.1175/JAS-D-19-0160.1, 2019.

Schumann, U., Konopka, P., Baumann, R., Busen, R., Gerz, T., Schlager, H., Schulte, P., and Volkert, H.: Estimate of diffusion parameters of aircraft exhaust plumes near the tropopause from nitric oxide and turbulence measurements, Journal of Geophysical Research: Atmospheres, 100, 14 147–14 162, https://doi.org/https://doi.org/10.1029/95JD01277, 1995.

Sharman, R. D. and Lane, T., eds.: Aviation Turbulence: Processes, Detection, Prediction, Springer, https://doi.org/10.1007/978-3-319-23630-8, 2016.

https://doi.org/10.5194/egusphere-2026-2628
Preprint. Discussion started: 29 May 2026

Sharman, R. D. and Trier, S. B.: Influences of Gravity Waves on Convectively Induced Turbulence (CIT): A Review, Pure Appl. Geophys., 176, 1923 – 1958, https://doi.org/https://doi.org/10.1007/s00024-018-1849-2, 2019.

Sharman, R. D., Doyle, J. D., and Shapiro, M. A.: An Investigation of a Commercial Aircraft Encounter with Severe Clear-Air Turbulence over Western Greenland, Journal of Applied Meteorology and Climatology, 51, 42 – 53, https://doi.org/10.1175/JAMC-D-11-044.1, 2012.

Sharman, R. D., Cornman, L. B., Meymaris, G., Pearson, J., and Farrar, T.: Description and Derived Climatologies of Automated In Situ Eddy-Dissipation-Rate Reports of Atmospheric Turbulence, Journal of Applied Meteorology and Climatology, 53, 1416 – 1432, https://doi.org/10.1175/JAMC-D-13-0329.1, 2014.

Shepard, D.: A two-dimensional interpolation function for irregularly-spaced data, in: Proceedings of the 1968 23rd ACM national conference, pp. 517–524, 1968.

Stephan, C. C. and Stevens, B.: Dynamical imprints on precipitation cluster statistics across a hierarchy of high-resolution simulations, Atmospheric Chemistry and Physics, 25, 1209–1226, https://doi.org/10.5194/acp-25-1209-2025, 2025.

Stevens, B., Ament, F., Bony, S., Crewell, S., Ewald, F., Gross, S., Hansen, A., Hirsch, L., Jacob, M., Kölling, T., Konow, H., Mayer, B., Wendisch, M., Wirth, M., Wolf, K., Bakan, S., Bauer-Pfundstein, M., Brueck, M., Delanoë, J., Ehrlich, A., Farrell, D., Forde, M., Gödde, F., Grob, H., Hagen, M., Jäkel, E., Jansen, F., Klepp, C., Klingebiel, M., Mech, M., Peters, G., Rapp, M., Wing, A. A., and Zinner, T.: A High-Altitude Long-Range Aircraft Configured as a Cloud Observatory: The NARVAL Expeditions, Bulletin of the American Meteorological Society, 100, 1061 – 1077, https://doi.org/10.1175/BAMS-D-18-0198.1, 2019.

Stevens, B., Bony, S., Farrell, D., Ament, F., Blyth, A., Fairall, C., Karstensen, J., Quinn, P. K., Speich, S., Acquistapace, C., Aemisegger, F., Albright, A. L., Bellenger, H., Bodenschatz, E., Caesar, K.-A., Chewitt-Lucas, R., de Boer, G., Delanoë, J., Denby, L., Ewald, F., Fildier, B., Forde, M., George, G., Gross, S., Hagen, M., Hausold, A., Heywood, K. J., Hirsch, L., Jacob, M., Jansen, F., Kinne, S., Klocke, D., Kölling, T., Konow, H., Lothon, M., Mohr, W., Naumann, A. K., Nuijens, L., Olivier, L., Pincus, R., Pöhlker, M., Reverdin, G., Roberts, G., Schnitt, S., Schulz, H., Siebesma, A. P., Stephan, C. C., Sullivan, P., Touzé-Peiffer, L., Vial, J., Vogel, R., Zuidema, P., Alexander, N., Alves, L., Arixi, S., Asmath, H., Bagheri, G., Baier, K., Bailey, A., Baranowski, D., Baron, A., Barrau, S., Barrett, P. A., Batier, F., Behrendt, A., Bendinger, A., Beucher, F., Bigorre, S., Blades, E., Blossey, P., Bock, O., Böing, S., Bosser, P., Bourras, D., Bouruet-Aubertot, P., Bower, K., Branellec, P., Branger, H., Brennek, M., Brewer, A., Brilouet, P.-E., Brügmann, B., Buehler, S. A., Burke, E., Burton, R., Calmer, R., Canonici, J.-C., Carton, X., Cato Jr., G., Charles, J. A., Chazette, P., Chen, Y., Chilinski, M. T., Choularton, T., Chuang, P., Clarke, S., Coe, H., Cornet, C., Coutris, P., Couvreux, F., Crewell, S., Cronin, T., Cui, Z., Cuypers, Y., Daley, A., Damerell, G. M., Dauhut, T., Deneke, H., Desbios, J.-P., Dörner, S., Donner, S., Douet, V., Drushka, K., Dütsch, M., Ehrlich, A., Emanuel, K., Emmanouilidis, A., Etienne, J.-C., Etienne-Leblanc, S., Faure, G., Feingold, G., Ferrero, L., Fix, A., Flamant, C., Flatau, P. J., Foltz, G. R., Forster, L., Furtuna, I., Gadian, A., Galewsky, J., Gallagher, M., Gallimore, P., Gaston, C., Gentemann, C., Geyskens, N., Giez, A., Gollop, J., Gouirand, I., Gourbeyre, C., de Graaf, D., de Groot, G. E., Grosz, R., Güttler, J., Gutleben, M., Hall, K., Harris, G., Helfer, K. C., Henze, D., Herbert, C., Holanda, B., Ibanez-Landeta, A., Intrieri, J., Iyer, S., Julien, F., Kalesse, H., Kazil, J., Kellman, A., Kidane, A. T., Kirchner, U., Klingebiel, M., Körner, M., Kremper, L. A., Kretzschmar, J., Krüger, O., Kumala, W., Kurz, A., L'Hégaret, P., Labaste, M., Lachlan-Cope, T., Laing, A., Landschützer, P., Lang, T., Lange, D., Lange, I., Laplace, C., Lavik, G., Laxenaire, R., Le Bihan, C., Leandro, M., Lefevre, N., Lena, M., Lenschow, D., Li, Q., Lloyd, G., Los, S., Losi, N., Lovell, O., Luneau, C., Makuch, P., Malinowski, S., Manta, G., Marinou, E., Marsden, N., Masson, S., Maury, N., Mayer, B., Mayers-Als, M., Mazel, C., McGeary, W., McWilliams, J. C., Mech, M., Mehlmann, M., Meroni, A. N., Mieslinger, T., Minikin, A., Minnett, P., Möller, G., Morfa Avalos, Y., Muller, C., Musat, I., Napoli, A., Neuberger, A., Noisel, C., Noone, D., Nordsiek, F., Nowak, J. L., Oswald, L., Parker, D. J., Peck, C., Person, R., Philippi, M., Plueddemann, A., Pöhlker, C., Pörtge, V., Pöschl, U., Pologne, L., Posyniak, M., Prange, M., Quiñones Meléndez, E., Radtke, J., Ramage,

https://doi.org/10.5194/egusphere-2026-2628
Preprint. Discussion started: 29 May 2026

K., Reimann, J., Renault, L., Reus, K., Reyes, A., Ribbe, J., Ringel, M., Ritschel, M., Rocha, C. B., Rochetin, N., Röttenbacher, J., Rollo, C., Royer, H., Sadoulet, P., Saffin, L., Sandiford, S., Sandu, I., Schäfer, M., Schemann, V., Schirmacher, I., Schlenczek, O., Schmidt, J., Schröder, M., Schwarzenboeck, A., Sealy, A., Senff, C. J., Serikov, I., Shohan, S., Siddle, E., Smirnov, A., Späth, F., Spooner, B., Stolla, M. K., Szkółka, W., de Szoeke, S. P., Tarot, S., Tetoni, E., Thompson, E., Thomson, J., Tomassini, L., Totems, J., Ubele, A. A., Villiger, L., von Arx, J., Wagner, T., Walther, A., Webber, B., Wendisch, M., Whitehall, S., Wiltshire, A., Wing, A. A., Wirth, M., Wiskandt, J., Wolf, K., Worbes, L., Wright, E., Wulfmeyer, V., Young, S., Zhang, C., Zhang, D., Ziemen, F., Zinner, T., and Zöger, M.: EUREC^{4}A, Earth System Science Data, 13, 4067–4119, https://doi.org/10.5194/essd-13-4067-2021, 2021.

Stevens, B., Bony, S., Gross, S., Klocke, D., Windmiller, J. M., Wing, A. A., von Bismarck, J., Brito, E., David, R. O., Delanoë, J., Farrell, D., and Wu, Y.: ORCESTRA: Organized Convection and EarthCARE Studies Over the Tropical Atlantic, Tellus, https://doi.org/10.16993/tellus.4123, 2026.

Strauss, L., Serafin, S., Haimov, S., and Grubišić, V.: Turbulence in breaking mountain waves and atmospheric rotors estimated from airborne in situ and Doppler radar measurements, Quarterly Journal of the Royal Meteorological Society, 141, 3207–3225, https://doi.org/https://doi.org/10.1002/qj.2604, 2015.

Tegtmeier, S., Anstey, J., Davis, S., Dragani, R., Harada, Y., Ivanciu, I., Pilch Kedzierski, R., Krüger, K., Legras, B., Long, C., Wang, J. S., Wargan, K., and Wright, J. S.: Temperature and tropopause characteristics from reanalyses data in the tropical tropopause layer, Atmospheric Chemistry and Physics, 20, 753–770, https://doi.org/10.5194/acp-20-753-2020, 2020.

Tennekes, H. and Lumley, J. L.: A First Course in Turbulence, MIT Press, 1 edn., 1972.

Trier, S. B., Sharman, R. D., Muñoz-Esparza, D., and Keller, T. L.: Effects of Distant Organized Convection on Forecasts of Widespread Clear-Air Turbulence, Monthly Weather Review, 150, 2593 – 2615, https://doi.org/10.1175/MWR-D-22-0077.1, 2022.

Vassilicos, J. C.: Dissipation in Turbulent Flows, Annual Review of Fluid Mechanics, 47, 95–114, https://doi.org/https://doi.org/10.1146/annurev-fluid-010814-014637, 2015.

Wacławczyk, M., Gozingan, A. S., Nzotungishaka, J., Mohammadi, M., and P. Malinowski, S.: Comparison of Different Techniques to Calculate Properties of Atmospheric Turbulence from Low-Resolution Data, Atmosphere, 11, https://doi.org/10.3390/atmos11020199, 2020.

Wacławczyk, M., Nzotungishaka, J., Jędrejko, P., Sarkar, J., and Malinowski, S. P.: Dissipation Scaling with a Variable C_ϵ Coefficient in the Stable Atmospheric Boundary Layer, Atmosphere, 16, https://doi.org/10.3390/atmos16020188, 2025.

Wang, K.-Y.: Severe turbulence from deep convective clouds during flight SQ321 on 21 May 2024, Scientific Reports, 15, 29 923, https://doi.org/https://doi.org/10.1038/s41598-025-15905-w, 2025.

White, F. M.: Viscous Fluid Flow, McGraw-Hill New York, 2 edn., 1991.

Wilms, H., Bramberger, M., and Dörnbrack, A.: Observation and simulation of mountain wave turbulence above Iceland: Turbulence intensification due to wave interference, Quarterly Journal of the Royal Meteorological Society, 146, 3326–3346, https://doi.org/https://doi.org/10.1002/qj.3848, 2020.

Windmiller, J. M.: The Calm and Variable Inner Life of the Atlantic Intertropical Convergence Zone: The Relationship Between the Doldrums and Surface Convergence, Geophysical Research Letters, 51, e2024GL109 460, https://doi.org/https://doi.org/10.1029/2024GL109460, e2024GL109460 2024GL109460, 2024.

Windmiller, J. M. and Stevens, B.: The inner life of the Atlantic Intertropical Convergence Zone, Quarterly Journal of the Royal Meteorological Society, 150, 523–543, https://doi.org/https://doi.org/10.1002/qj.4610, 2024.

https://doi.org/10.5194/egusphere-2026-2628
Preprint. Discussion started: 29 May 2026

Woiwode, W., Dörnbrack, A., Geldenhuys, M., Friedl-Vallon, F., Giez, A., Gulde, T., Höpfner, M., Johansson, S., Kaifler, B., Kleinert, A., Krasauskas, L., Kretschmer, E., Maucher, G., Neubert, T., Nordmeyer, H., Piesch, C., Preusse, P., Rapp, M., Riese, M., Schumann, U., and Ungermann, J.: Non-Orographic Gravity Waves and Turbulence Caused by Merging Jet Streams, Journal of Geophysical Research: Atmospheres, 128, e2022JD038 097, https://doi.org/https://doi.org/10.1029/2022JD038097, e2022JD038097 2022JD038097, 2023.

Xie, P., Joyce, R., Wu, S., Yoo, S.-H., Yarosh, Y., Sun, F., and Lin, R.: Reprocessed, Bias-Corrected CMORPH Global High-Resolution Precipitation Estimates from 1998, Journal of Hydrometeorology, 18, 1617 – 1641, https://doi.org/10.1175/JHM-D-16-0168.1, 2017.

Xie, P., Joyce, R., Wu, S., Yoo, S.-H., Yarosh, Y., Sun, F., and Lin, R.: NOAA CDR Program, NOAA Climate Data Record (CDR) of CPC Morphing Technique (CMORPH) High Resolution Global Precipitation Estimates, Version 1 30 min 8 km, NOAA National Centers for Environmental Information, https://doi.org/https://doi.org/10.25921/w9va-q159, 2019.